

**FACILITATED CHARACTERIZATION OF A CATALYTIC  
PARTIAL OXIDATION FUEL REFORMER USING IN SITU  
MEASUREMENTS**

A Thesis  
Presented to  
The Academic Faculty

by

Dimitri Hughes

In Partial Fulfillment  
of the Requirements for the Degree  
Master of Science in the  
School of Mechanical Engineering

Georgia Institute of Technology  
December 2009

**COPYRIGHT 2009 BY DIMITRI HUGHES**

**FACILITATED CHARACTERIZATION OF A CATALYTIC  
PARTIAL OXIDATION FUEL REFORMER USING IN SITU  
MEASUREMENTS**

Approved by:

Dr. Comas L. Haynes, Co-Advisor  
Georgia Tech Center for Innovative Fuel Cell and Battery Technologies  
*Georgia Tech Research Institute*

Dr. William J. Wepfer, Co-Advisor  
School of Mechanical Engineering  
*Georgia Institute of Technology*

Dr. Sheldon M. Jeter  
School of Mechanical Engineering  
*Georgia Institute of Technology*

Date Approved: November 10, 2009

## ACKNOWLEDGEMENTS

I would first like to thank Dr. Comas Haynes for his technical support and guidance with this research project and throughout my graduate studies. I would also like to thank the other members of my reading committee, co-advisor and school chair Dr. William Wepfer and Dr. Sheldon Jeter for their assistance in completing this milestone.

To my group members, J. Chris Ford, Kevin Davies, and Dr. George Nelson, I extend much gratitude and appreciation for all of your support, personally, professionally and technically, to this point and continuing forward. To the members of the Georgia Institute of Technology chapter of the Black Graduate Student Association, you have been one of, if not the most integral part of my graduate school process. Thank you for the friendships, thank you for making it memorable, and thank you so much for your support, guidance, social outlets, love and care.

To my mother, Wenora Hughes, for always pushing me and supporting me through all of my academic and life pursuits. I would not have made it this far without you and I owe so much of my success to your love, care, and mothering. To ZHRAA, thank you for the love, the brotherhood, the support, and the interest and care. Thank you for making excellence the standard and for equating excellence to changing the world. To Christina, you played a significant and necessary role in both my personal and spiritual development throughout my time at Georgia Tech. I extend the utmost appreciation and gratitude and wish you many blessings in your new endeavor. And to Joyette Mitchell, your love is felt continually and your support is constant and evident. Thank you for the daily fuel that you provide me in making it through each day of this process. I love you.

# TABLE OF CONTENTS

	Page
ACKNOWLEDGEMENTS	iii
LIST OF TABLES	vii
LIST OF FIGURES	viii
NOMENCLATURE	x
LIST OF ABBREVIATIONS	xi
SUMMARY	xii
<u>CHAPTER</u>	
1 Introduction	1
1.1 Fuel Reformer Technology Overview	1
1.2 Fuel Reformer Applications	5
1.3 Importance of Reformer Characterization	6
1.4 Novelty of in situ Measurements for Facilitating Thermodynamic Analysis	8
1.5 Results Summary	10
2 Literature Review	12
2.1 Introduction	12
2.2 Computational Reformer Literature	14
2.3 Experimental Reformer Literature	18
2.4 SpaciMS Literature	23
2.5 Conclusion	25
3 Experimental Set-Up	26
3.1 SpaciMS Validation	26

3.1.1 Gas Phase Reaction Analysis	27
3.1.1.1 Experimental Set-Up	28
3.1.1.2 Results	30
3.2 Instrumentation Development	40
3.2.1 Translation Stage	41
3.2.1.1 Thermocouple Stage	41
3.2.1.2 SpaciMS Capillary Stage	43
3.3 Bench Flow Reactor Set-Up	45
4 Experimental Results Discussion	48
4.1 Temperature Analysis Results	48
4.2 SpaciMS Results	52
5 Computational Model Development	59
5.1 Qualitative Analysis	59
5.1.1 Engineering Equation Solver Justification	59
5.1.2 EES Code Development Methodology	60
5.2 Quantitative Analysis	66
5.2.1 1 <sup>st</sup> Law Analysis	66
6 Conclusion	69
6.1 Summary of Results	69
6.2 Computational Challenges	72
6.2.1 Reaction Kinetics	72
6.2.2 2 <sup>nd</sup> Law Analysis	73
6.3 Future Work	73
APPENDIX A: EES Thermodynamic Analysis Code	76
APPENDIX B: Ideal Gas Law Approximation	79

APPENDIX C: Supplemental SpaciMS Plots	82
REFERENCES	84

## LIST OF TABLES

	Page
Table 3.1: Intra-Catalyst gas phase reaction results	39
Table 4.1: Peak temperature location for given space velocities	50
Table 5.1: Space velocity with corresponding standardized volumetric flow rates	63
Table 5.2: Space velocity with corresponding mass flow rates	65
Table B.1: Compressibility factor solutions	80

## LIST OF FIGURES

	Page
Figure 1.1: Internal reforming schematic for fuel cell application	1
Figure 1.2: External reforming schematic for fuel cell application	2
Figure 1.3: Fuel processing flow chart	3
Figure 1.4: CPOx honeycomb monolith catalyst – top view	5
Figure 1.5: SpaciMS	9
Figure 3.1: Intra-capillary gas phase reaction analysis experimental set-up for 12 inch heated zone	29
Figure 3.2: Intra-capillary gas phase reaction analysis set-up schematic for 1.7035 inch heated zone	30
Figure 3.3: Intra-capillary gas phase reaction profile for inlet fuel mixture (a) as a function of temperature for the 12 inch heated zone	33
Figure 3.4: Intra-capillary gas phase reaction profile for inlet fuel mixture (a) as a function of temperature for the 1.7035 inch heated zone	34
Figure 3.5 Intra-capillary gas phase reaction profile for outlet syn gas mixture (b) as a function of temperature for a 12 inch heated zone	36
Figure 3.6 Intra-Capillary gas phase reaction profile for steam methane reforming mixture (c) as a function of temperature for a 1.7035 inch heated zone	37
Figure 3.7 Bench flow reactor quartz tube assembly - Intra-catalyst gas phase reaction analysis	38
Figure 3.8: Thermocouple translation stage	42
Figure 3.9: SpaciMS capillary translation stage	43
Figure 3.10: Bench flow reactor quartz tube assembly	45
Figure 4.1: Temperature vs. Position as a function of space velocity	49
Figure 4.2: Species composition as a function of position for 75k hr <sup>-1</sup> experiment	54
Figure 4.3: Species composition as a function of position for 150k hr <sup>-1</sup> experiment	56
Figure 4.4: Hydrogen concentration as a function of position across all space	57



## Velocities

Figure 4.5: Methane concentration as a function of position across all space velocities	58
Figure 5.1: CPOx honeycomb monolith catalyst – top view	61
Figure 5.2: Data acquisition discretization schematic	63
Figure 5.3: Heat released vs. Position normalized by fuel flow	70
Figure C.1: Species composition as a function of position for 47k hr <sup>-1</sup> experiment	82
Figure C.2: Species composition as a function of position for 100k hr <sup>-1</sup> experiment	82
Figure C.3: Carbon Monoxide concentration as a function of position across all space velocities	83
Figure C.4: Methane concentration as a function of position across all space velocities	83

## NOMENCLATURE

$\dot{Q}$	Heat released
$\dot{m}$	Mass flow rate
$\dot{n}$	Molar flow rate
$h$	Enthalpy
$\dot{V}$	Volumetric Flow Rate
$\mu$	Molar mass
$T$	Temperature
$P$	Pressure
$R$	Gas Constant
$v$	Specific Volume
$x$	Mole Fraction
$\sigma$	Standard Deviation
Recurring Subscripts	
$std$	Standard conditions
$actual$	Actual conditions
$in$	Inlet
$out$	Outlet

## LIST OF ABBREVIATIONS

APU	Auxiliary Power Unit
AMU	Atomic Mass Unit
BFR	Bench Flow Reactor
CPO <sub>x</sub>	Catalytic Partial Oxidation
FTI	Feed Temperature Increase
PEMFC	Proton Electron Membrane Fuel Cell
PO <sub>x</sub>	Partial Oxidation
RF	Reverse Flow
SpaciMS	Spatially Resolved Capillary Inlet Mass Spectrometry
SOFC	Solid Oxide Fuel Cell
UD	Uni-Directional

## SUMMARY

Hydrocarbon conversion and synthesis gas production are two components of the power production process that require significant development and exploration in the advanced energy arena. To remain within our current fueling infrastructure, it is imperative that an efficient and reliable mechanism to facilitate these components of the power production process is developed for automotive applications. A honeycomb monolith rhodium based catalyst has been identified as a potential fuel reformer element for use in automotive hydrocarbon fuel conversion. Using the novel and minimally invasive SpaciMS (Spatially resolved capillary inlet Mass Spectroscopy), developed at Oak Ridge National Laboratories, and an internal temperature acquisition system, the impact of fuel inlet space velocity on the operating rhodium based catalytic fuel reformer of interest was parametrically studied. In situ temperature and species profiles of the catalyst during steady state operation were produced. The data acquired through these experiments was then used to demonstrate analytic capability by conducting thermodynamic analyses on the operating fuel reformer. Experimental and analytical results can be used in development of design considerations for fuel conversion systems.

# CHAPTER 1

## INTRODUCTION

### 1.1 Fuel Reformer Technology Overview

Fuel reforming is a method for producing a mixture of hydrogen ( $H_2$ ) and carbon monoxide (CO), more commonly referred to as synthesis gas or syngas, from hydrocarbon fuels. There are two major types of reforming in the power system arena, and they are internal reforming and external reforming.

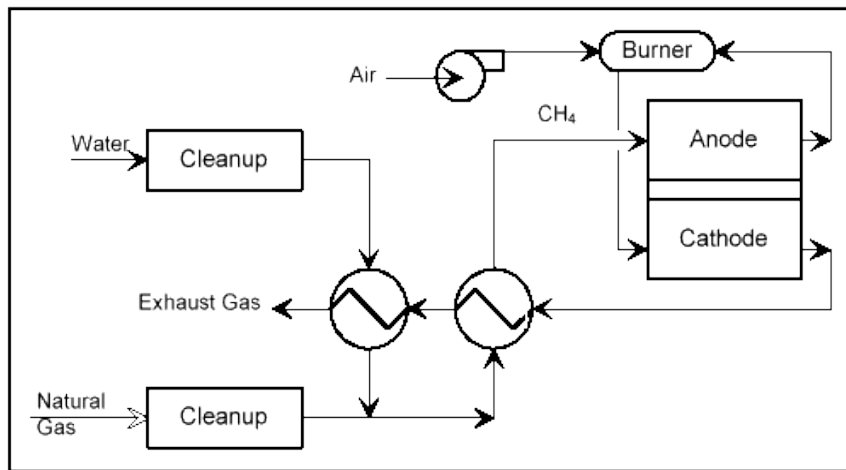
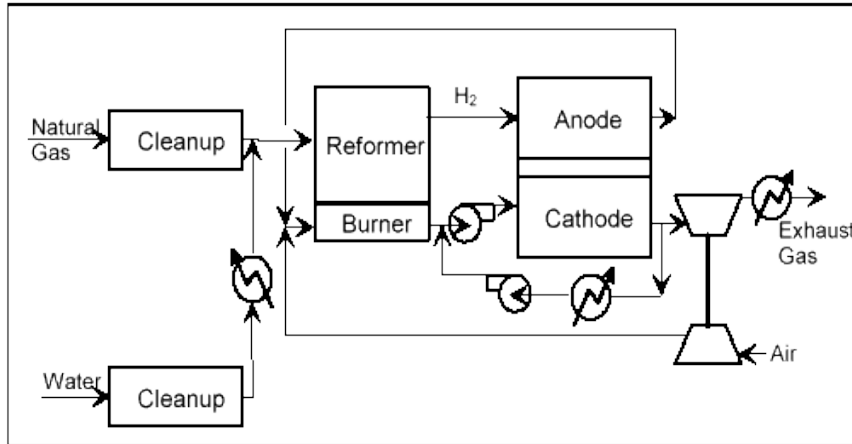


Figure 1.1 Internal reforming schematic for fuel cell application<sup>1</sup>

Figures 1.1 and 1.2 illustrate the difference between internal and external reforming as it applies to fuel cell applications. As illustrated in Figure 1.1, the natural gas mixture is sent directly to the fuel cell anode after it exits the cleaning component. The fuel cell anode material is actually comprised of a catalyst that can convert the inlet natural gas into fuel (i.e.  $H_2$ , and CO, along with other byproducts) that can be used for

<sup>1</sup> <http://hydrogencommerce.com/FCHandbook/TechOver1-1FCDesc.htm>

power production by the fuel cell. Figure 1.2 illustrates a reformer assembly, external from the fuel cell, which is responsible for converting the natural gas into consumable fuel, which is then fed to the fuel cell.



**Figure 1.2 External reforming schematic for fuel cell application<sup>1</sup>**

The difference between internal and external reforming is determined by the location of the reformation process relative to the power-producing device. When the fuel is reformed within the confines of the actual power producing device it is referred to as internal reforming, and when it is processed externally from the device it is known as external reforming

A major component in any fuel cell system is a fuel processor, which includes a fuel reformer. The fuel processor is used to convert the inlet fuel to a form that can be used to power the fuel cell, or any other applicable power system. Figure 1.3 presents a general fuel processing flow diagram. As illustrated, there are three main steps in the fuel processing process: desulphurization, reformation and purification. All three of these processes work dynamically to produce H<sub>2</sub> and/or CO for fuel cell consumption. The reformation process is the one of particular interest for this research project.

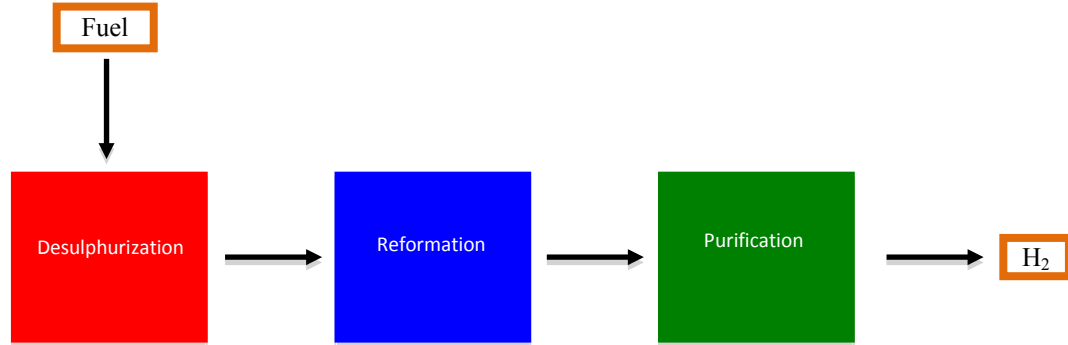


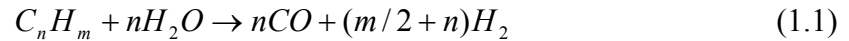
Figure 1.3 Fuel processing flow chart<sup>2</sup>

External reforming is most applicable to fuel cell systems. Certain fuel cells that operate at higher temperatures (i.e. solid oxide fuel cells, molten carbonate fuel cells) are capable of reforming the fuel inside the fuel cell stack prior to consumption and power production. This is called internal reforming, wherein systems are designed to convert inlet fuel into a consumable form without an adjacent external system. External reforming is conducted through a device, separate from the power generation system. The sole purpose of an external reformer is to convert fuel into a form that can be utilized by the power generation device. External reformers are typically constructed from some substrate material and coated with a catalyst material (often noble metal), which is utilized to facilitate the necessary reactions to produce synthesis gas. Fuel reformers can be used to convert any type of hydrocarbon fuel (gasoline, diesel, natural gas, propane, etc.) into H<sub>2</sub> and CO. The external reformer of study for this project is specifically being utilized for the reformation of methane gas, the major constituent in natural gas.

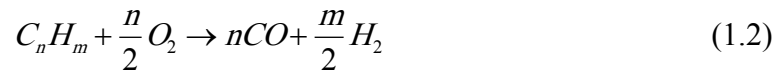
There are three major types of reforming technologies: steam reforming, partial oxidation reforming and auto thermal reforming. In steam reforming, the fuel stream is

<sup>2</sup> <http://www.eifer.uni-karlsruhe.de/194.php>

mixed with steam in the presence of a catalyst to produce synthesis gas. To date, steam reformation is the most highly developed and most efficient of the reformation technologies [1]. The general chemical equation illustrating steam reformation is exhibited in equation 1.



In partial oxidation (POX), the fuel source is combined with sub-stoichiometric oxygen or air to liberate hydrogen. The process is not as efficient as steam reformation but it is highly exothermic and thus can be initiated through combustion leading to quick start up. The general chemical equation illustrating partial oxidation is exhibited in equation 2.



Autothermal reformation is a combination of steam reformation and POX fuel processing. By leveraging the quick start up and exothermic nature of POX with the endothermic nature of steam reformation, the reformer can be started and operated in self-sustained manner

The reformer of interest for the present research is a honeycomb monolith, rhodium-based partial oxidation fuel reformer. The cylindrical honeycomb reformer is 1 inch long and 0.8 inches in outer diameter consisting of approximately 100 flow channels that have an approximate cross sectional area of 0.5 in<sup>2</sup>. The catalyst is illustrated below in Figure 1.4. The fuel of interest for this research project was methane. Inlet gas



mixtures of methane and oxygen were balanced with either nitrogen or argon, because of their inert nature. These “feedstocks” were fed to the reactor and outlet streams of syngas with either nitrogen or argon were collected and analyzed at the outlet. Species and temperature profiles of the reformer operating as steady state were created using the Spatially resolved capillary inlet Mass Spectrometry system (SpaciMS) developed at Oak Ridge National Laboratories in Oak Ridge, TN. Minimally invasive temperature acquisition mechanisms were developed within the same facility.

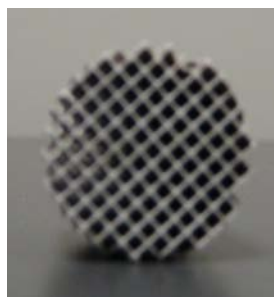


**Figure 1.4: CPOx honeycomb monolith catalyst – top view  
(Note: Also Figure 5.1)**

## **1.2 Fuel Reformer Applications**

This new arena of fuel reformer research is centered on two specific applications: automotive emission control and auxiliary power units. Fuel reformers offer an effective way to decrease harmful emissions from fossil fuel powered automobiles, and provide a pathway to improve vehicle efficiency. Auxiliary power units (APUs) are free standing devices that are capable of generating power for purposes besides vehicle propulsion. Fuel reformers combined with fuel cells can serve as the heart of APUs that can be used in a variety of sectors.

Utilizing fuel reformers in hydrocarbon fuel powered vehicles allows the current fueling infrastructure to remain in place while integrating hydrogen-powered components.

The ability to produce hydrogen on-board the vehicle as opposed to it being produced externally and fed directly to the power system is what makes the use of fuel reformers so novel. On-board fuel reformation eliminates the development of hydrogen storage components for vehicles, allows the pre-existing fuel infrastructure to remain in place and offers an efficient and effective methodology for hydrogen production. Though promising, sizing, scalability, system clean up, maintenance, and thermal management are just a few of design challenges that need to be addressed prior to technological integration.

Auxiliary power units or APUs convert energy for functions other than propulsion. APUs, driven by truck engines, consume over 800 million gallons of diesel fuel and cost the trucking industry close to \$2 billion per year. Currently, long haul trucks are required to idle for extended periods of time to keep their truck cabins' temperature controlled during required rest periods [1,2]. The EPA is currently promoting the production of many idle reduction technologies that can be integrated into long haul truck power and emission control systems. With syngas being the fuel mixture for solid oxide fuel cells (SOFC), and fuel reformers offering an efficient and effective way to produce syngas, a SOFC is a very viable candidate for an APU power system. Employing the use of APUs in the residential and commercial electrical power arenas has been discussed as well. Free standing APUs in neighborhoods or in commercial districts will make electrical power more reliable. Electrical power systems will be less susceptible to outages and failures thus decreasing and possibly eliminating the dependence for overhead and underground wires.

### **1.3 Importance of Reformer Characterization**

The primary applications that are being suggested for fuel reforming technology require a high level of dependability. Integrating fuel reformers into automotive propulsion systems and APUs will require a holistic understanding of the operation of a reformer. Characterizing the thermal phenomena and reaction rate kinetics along the length of the reactor is a necessary contribution to achieving this level of understanding.

Empirical data shows an extremely elevated temperature at the front of the reactor, with a gradual decrease in temperature as the outlet is approached. This is expected due to the highly exothermic nature of the reactions taking place in the oxidation zone and the endothermic nature of the reactions taking place in the reformation zone. Significant temperature gradients can impact performance, reliability and durability of a given device [3,4]. This thesis provides in situ temperature and thermodynamic data that not only characterizes and quantifies the temperature gradients that exist within the reformer but also provides insight into identifying areas of localized heat generation and chemical phenomena.

The catalyst coating on the substrate strongly influences fuel reformation. It allows the reaction of hydrocarbon fuel, in this particular case methane, to begin at a relatively modest temperature and thus propels the reformation of the fuel. It is known that over time, a catalyst coating can degrade and eventually become inactive. The rate of degradation of the emphasized rhodium catalyst wash coat over the honeycomb monolith substrate plays a significant role in determining the lifetime of this given reformer, and thus the power system that it serves. Though this project is not an analysis on the lifetime of catalytic partial oxidation fuel reformers, the facilitated characterization of reaction

rate kinetics along the reactor that is attempted is a significant piece to determining the rate of catalyst degradation and thus the lifetime of these reformers.

The computational tool that has been developed is designed to conduct 1st law thermodynamic analysis with the capability to conduct 2<sup>nd</sup> law analysis along discretized portions of the reformer. The first law analysis will illustrate the heat generation or consumption along the reactor due to the chemical reactions taking place. The second law analysis, once the necessary operating parameters are obtained (i.e. boundary temperature profile), will illustrate entropy generation and exergy destruction along the reformer due to the internal activity.

#### **1.4 Novelty of in situ Measurements for Facilitating Thermodynamic Analysis**

Much like fuel cells have been for the majority of their lifetime, fuel reformers have long been limited to the realm of “black box” analysis (i.e., it was one of those systems wherein one could analyze inlet and outlet states, but the ability to determine the internal phenomena of the system appeared inaccessible). Oak Ridge National Laboratories has made a major step in taking both fuel cells and fuel reformers out of the black box analysis arena. The development of the spatially resolved capillary-inlet mass spectrometry system, coined SpaciMS, has allowed investigators to make minimally invasive, in situ measurements of various power systems.



**Figure 1.5: SpaciMS**

SpaciMS, illustrated partially in Figure 1.4, is a mass spectrometer whose sampling capillaries are on the order of  $50\mu\text{m}$ -  $150\mu\text{m}$  in diameter. The sampling capillaries are constructed of quartz and covered with a polymer coating, which makes the capillaries very flexible. As a testament to its invasive nature, in an experiment conducted in 2005, a set of intra fuel cell stack measurements were made that utilized the SpaciMS system [5].

During the summer of 2006, collaboration with Oak Ridge National Laboratories and the Haynes research group at Georgia Tech resulted in the in situ characterization of an operating rhodium based partial oxidation fuel reformer. Along with utilizing the SpaciMS system, a minimally invasive in situ temperature acquisition system was developed. Coupling these systems provided the capability to develop profiles of temperature and species concentration variations along the reformer.

Use of in situ measurements is extremely novel and using them to conduct thermodynamic and chemical kinetic analysis has not yet been heavily explored. The present thesis documents how tools and instrumentation necessary for *in situ* analysis of fuel reformers have been developed in conjunction with ORNL colleagues and proven

valid; and subsequent computational work has been used to resolve thermal phenomena within a candidate autothermal fuel processor. This research project endeavored to develop and validate the use of a minimally invasive data acquisition mechanism and use that mechanism to characterize an operating partial oxidation fuel reformer from both an empirical and analytical framework.

### **1.5 Results Summary**

Utilizing the in situ diagnostic system developed in-house at Oak Ridge National Laboratories, the impact of fuel stream space velocity on an operating rhodium based partial oxidation fuel reformer was empirically investigated. For the sake of this investigation, space velocity is used to quantify fuel flow through the reactor. The space velocity is equal to the volumetric flow of feed flowing through a given reactor divided by the volume of said reactor. Typically used in chemical reactor analysis, space velocity indicates how many reactor volumes of feed can be treated per unit time, hence the unit  $\text{time}^{-1}$ . The unit  $\text{k hr}^{-1}$  signifies thousands of inverse hours. Fuel stream space velocities ranging between  $47 \text{ k hr}^{-1}$  and  $150 \text{ k hr}^{-1}$  were studied in this investigation. Utilizing the systems capabilities, in situ temperature and species profiles were produced.

Results exhibit a significant impact of space velocity on reformer operation. The start position and length of the reaction zone (length of catalyst occupied by constituents) increases with increased space velocity. Space velocity also had an impact on the axial location of complete fuel conversion. The axial location of complete fuel conversion to the desired syngas mixture moved further down stream with increased space velocities.

Empirical data showed an increased downstream inflection in the species profiles of the constituents that serve as reactants for the methanation reaction. It is believed that space velocity had an impact on the presence of the methanation reaction down stream. No definitive conclusions could be made.

Thermodynamic analysis utilizing this empirical data exhibited the presence of significant localized heat generation corresponding with the reaction zone. Generally, heat generated and axial location down the reactor length increased with space velocity. A maximum local heat generation, however, is observed for the  $100 \text{ k hr}^{-1}$  space velocity case. It is believed that this deviation from the expected general is due to some experimental error or discretization issue in the computational analysis. The experiment and analysis needs to be conducted in a repeated fashion in order to validate this claim.

The instrumentation to acquire internal operating diagnostics of a fuel reformer, and other essential power system components, was constructed, tested and validated. The data acquired was used to conduct quantitative thermodynamic analysis on an operating fuel reformer and information for potential design considerations was produced.

## **Chapter 2**

### **LITERATURE REVIEW**

#### **2.1 Introduction**

The focus of this thesis project is to utilize novel in situ measurements to analyze and characterize a rhodium-based partial oxidation fuel reformer. This approach to investigating this reformer system is divided into two components: computational model development and data characterization and empirical analysis. This literature review focuses on examining each of these components. Section 2.2, entitled computational reformer literature, reviews the literature that presented methodologies for developing theoretical models of operating fuel reformers. Using a variety of approaches that are exhibited in the individual reviews, a number of the investigators were able to produce predictability mechanisms that were utilized to simulate operating reforming systems.

Section 2.3, entitled experimental reformer literature, reviews literature that focuses mainly on a purely empirical investigation of operating reformers. Some investigators focused on intra reactor measurements while others focused on parametric studies of reverse-flow (RF) and uni-directional (UD) reactors. All of the literature spoke on empirically validated trends in operating reformers and all of the sources qualitatively agreed.

Section 2.4, entitled SpaciMS literature, speaks to the validity and novel nature of the SpaciMS system that was developed at Oak Ridge National Laboratories. Since this system was used to acquire all in situ measurements for this project, literature validating the instrumentation was necessary for this investigation. The literature review relates primarily to a fuel cell application, but its applicability for this application is evident.



In an attempt to speak to the larger arena of hydrogen production and alternative power systems, an article analyzing the feasibility of developing a hydrogen economy is presented first.

Over the past decade or so, governments across the globe, especially the United States and European nations, have placed a major focus on addressing the energy crisis. A primary component of this focus is a plan to develop a hydrogen fueled world. Kreith and West [6] speak to the feasibility of this goal. Both political and technical in nature and tone, this article does have an underling bias against the formation of a hydrogen economy; nevertheless it offers some noteworthy insight to the feasibility of such a goal.

This article was intended to serve as a “cradle to grave” analysis of the current pathways to produce hydrogen, conversion of hydrogen fuel to heat or electricity, and the eventual utilization of that heat or electricity. There are four hydrogen production pathways discussed in this paper: hydrogen produced from 1.) fossil fuels via chemical reactions; 2.) fossil, nuclear and renewable resources via thermolysis; 3.) fossil, nuclear and renewable sources via electrolysis; 4.) renewable or nuclear sources that do not utilize thermolysis or electrolysis.

Every hydrogen conversion mechanism of significant merit, including the use of fuel reformers, was investigated. Reasons ranging from poor efficiency to increased carbon dioxide emissions to failed cost benefit analysis were presented as evidence to abandon the goal of developing a hydrogen economy. This exhibits the necessity to develop technologies that can address efficiency and emission control needs and that can be utilized within our preexisting infrastructure. Development of fuel reforming technology is a means of bridging an established fossil fuel infrastructure to promising

hydrogen-based applications such as fuel cells and broaches the capabilities, if properly utilized, to address efficiency and emission control issues.

## **2.2 Computational Reformer Literature**

Sampara et al. [7], outlines a methodology of modeling each reactor present in a fuel processing system. The fuel processing system of interest for this investigation included a steam reformer, a water gas shift reactor and a preferential oxidation reactor. Utilizing mass transfer fundamentals and power law reaction rate expressions, a one dimensional model that includes both the bulk mass transfer and phenomenological reaction rate expressions needed to model each device is described.

Numerical schemes, which would serve as the base of the model of each component, were developed utilizing mass transfer fundamentals and reaction rate expressions obtained from literature. A temperature profile along each reactor needed to be assumed as the reaction rate expressions require temperature as an input. Once these numerical, one-dimensional models were developed, theoretical parametric studies were conducted on each component of the fuel processing system with methanol serving as the fuel. Conversion rates, species concentrations, reactor length, catalyst loading, and heat loss were all explored in the parametric studies. The model proved to be suitable for simulating a fuel processing system. The authors also concluded that a similar model could be used for a variety of reactors, highlighting monoliths specifically. This model shows direct applicability to characterizing the POX monolith of interest for this project.

This investigation presents a useful approach to modeling these fuel processing systems, however the one-dimensional constraint and the need to assume a temperature

profile is an area of concern. It has been exhibited though current empirical studies with the SpaciMS and a minimally invasive temperature acquisition system, that many factors impact the temperature profile of a reactor, therefore, not having temperature resolution built into the numerical scheme can lessen the inherent fidelity of the approach.

Nevertheless, this article directly applies to the computational component of this project. Except for temperature, this tool is able to predict pertinent profiles along a reactor and study the effect that various independent variables have on fuel processor operation.

Chaniotis et al. [8] developed a model of a micro reformer for a fuel cell unit and used this model to optimize the performance of the reformer. The focus of the optimization is the production of  $H_2$  from  $CH_4$ , which was quantified by the yield of  $H_2$  (ratio of  $H_2$  produced over the theoretical maximum  $H_2$  produced). Similar to the fuel reformer of interest for this thesis project, the reformer that was modeled was also a monolith. Though the same type of reactor was examined, different approaches were taken. Chaniotis et al. examined only a single channel of the monolith, where this project investigates the entire reactor with a plug flow methodology.

Two modeling techniques were employed in this investigation, Surface Perfectly Stirred Reactor Model (SPSR) and the Navier-Stokes Equation Model. The SPSR model makes assumptions that allow it to focus more on the resolution of reaction rates whereas the Navier-Stokes model focuses more on transport phenomena. In order to optimize this reformer, an equivalence ratio variable was defined as the actual fuel/oxygen ratio to the stoichiometric fuel/oxygen ratio. After a number of parametric studies, it was determined that hydrogen production is strongly dependent upon the equivalence ratio. An

equivalence ratio of 0.6 – 1.0 showed high levels of hydrogen production with realistic operating conditions (velocity= $1\text{ms}^{-1}$  and inlet temperature= $875\text{K}$ ).

The single channel approach produced novel and insightful results in the analysis of optimizing micro reactors, however isolating single channels and making the necessary boundary condition assumptions could lose validity when attempting to analyze the entire reactor. Though this could prove challenging for future work, the investigation still offered considerable insight into the problem at hand, because it highlights variables that have a direct impact on productivity of reformer systems and can be utilized to explain some of the phenomena that is prevalent in the resulting data. The insights from this study will be utilized in the composition of the discussion of the SpaciMS and temperature data profiles in Chapter 4.

Lutz et al. [9] analyzes the thermodynamics of partial oxidation hydrogen production under two assumptions: global reaction balances and chemical equilibrium. The global reaction analysis assumes that the reaction goes to completion. This mode serves as a “best case” scenario and allows the thermal efficiency at the upper limit of fuel conversion efficiency to be examined. The chemical equilibrium assumption adds a level of complexity and adds temperature dependence as a necessary parameter. For this study, a fixed uniform temperature is assumed so that the impact of temperature through parametric studies can be evaluated.

The investigation shows that the chemical equilibrium assumption yielded more reliable results than the global reaction balance, but both assumptions show a decrease in efficiency for the reformation of larger hydrocarbons. It is also predicted that the efficiency of steam reformation with partial oxidation will be in the range of 40%-60%

and thermal efficiency decreases with decreasing C/O ratio. This trend is due to more fuel being consumed by oxidation as opposed to reformation.

As intended by the author, this paper did not research the chemical kinetics of this operating reactor. Inclusion of this in the investigation would have made this paper more applicable to this thesis topic but the thermodynamic analysis did offer some useful insight. The approach taken within the given thesis development was empirical in nature, analyzing heat generation along the reactor; and the robust thermodynamic analyses presented within this paper were applicable. The findings of this article will be referenced and employed in Chapter 5 when the thermodynamic analysis results are discussed.

Kaisare et al. [10,11] presents the development and use of a one-dimensional model for methane partial oxidation in a tubular microreactor. Both uni-directional (UD) and reverse-flow (RF) reactors were studied. The microreactor of interest consisted of four cylindrical channels, each 500 $\mu$ m in diameter containing Pt/13%-Rh catalyst. Employing heat and mass transfer and kinetic fundamentals, a system of differential algebraic equations were formulated and solved with DASPK software. In addition to the development of this numerical scheme, timescale analysis was conducted to determine the impact that individual processes had on the overall speed of the reformation.

Two simulations were conducted. One utilized what is known as the GOS model, which consisted of kinetic equations developed by Gosiewski et al. The second model is known as the NK model and is based off of kinetic expressions developed by Numaguchi, et al. Through these simulations and the accompanying parametric studies, it was generally concluded that the RF reactors were more productive than the UD reactors. Varying parameters such as inlet velocity, which improved H<sub>2</sub> production in a linear

fashion, inlet gas temperature, reactor length and heat loss all substantiated that RF reformers are more efficient and productive than UD reformers.

Though this paper series focused on differentiating RF and UD reformers, it offered some valuable insight on qualitative analysis of fuel reforming systems. Despite omitting from the model certain reactions that are believed to take place, RF reformers proved to be more effective in H<sub>2</sub> production. Though RF reformers proved to be more effective in the arena of H<sub>2</sub> production, UD reformers followed the same trends. The exploitation of thermal dynamics along the reactor is the key factor in the improved productivity of RF reactors. The methodology and results presented in this paper will be referenced in the discussion of the empirical results in Chapter 4 of this thesis.

### **2.3 Experimental Reformer Literature**

Bharadwaj et al. [12] presents an overview of the progression of catalytic partial oxidation technology. At this time, production of syngas was extremely important, for it boasted many applications in a number of chemical processes. Many syngas production methods such as steam reformation and autothermal reforming, had been employed but catalytic partial oxidation presents a greater advantage in terms of speed and cost. A new millisecond contact time reformer, based off of this technology, was explored and compared to pre-existing technologies.

Bharadwaj et al. offered 4 major insights into the reformation world. Reformers have transitioned from “wet” to “dry”, from “endothermic” to “exothermic”, decreased contact time from several seconds to milliseconds, and moved from large reactors to small simple reactors. This investigation also confirmed that rhodium was the catalyst of

choice, achieving 95% selectivities and 90% conversion rates. This paper served as the summation of reforming technology to this point and was the springboard for further technical research.

This article serves as a “grassroots” background literature for this project. It outlined all of the major reforming technologies, many of which are still being investigated today, commented on the direction of the field and offered significant insight on where the technology stood and significant components of it. This will mainly be used as fundamental base for the technology that is being explored and its information will mostly contribute to the introduction of the thesis as well as computational model development.

The work presented by Horn et al. [3] produces *in situ* measurements of a foam rhodium based fuel reformer facilitating the partial oxidation of methane ( $\text{CH}_4$ ), as well as profiles produced from numerical simulations performed with a 38 step surface mechanism using both a porous 2D-model with mass and heat transfer and a simple plug-flow model [Horn, et al.]. This article also broaches the existence of a two-zone model, with complete consumption of  $\text{O}_2$  taking place in what is coined the “Oxidation” zone and production of  $\text{CO}$  and  $\text{H}_2$  in what is coined the “Reformation” zone

The experimental side of this investigation explored the impact of fuel mixture (c)/O ratios and flow rate on reactor performance. For a fixed flow rate of  $5 \text{ l min}^{-1}$ , the C/O ratios of 0.7, 1.0 and 1.3 were examined. The empirical studies exhibit an elevated operating temperature for  $\text{C/O} = 0.7$  ( $\sim 1040^\circ\text{C}$ ) than for  $\text{C/O} = 1.0$  and  $1.3$  ( $\sim 810^\circ\text{C}$ );  $\text{O}_2$  conversion occurred 4 times faster at  $\text{C/O}=1.0$  than for  $\text{C/O}=0.7$  and  $1.3$ . A stoichiometric C/O ratio of 1.0, based upon the catalytic partial oxidation reaction, was chosen as a basis

to compare the profiles for total flow rates of  $5 \text{ l min}^{-1}$  and  $10 \text{ l min}^{-1}$ . Both species profiles look qualitatively similar. The axial position at which total oxygen conversion is observed is located twice as far down the reactor length from the catalyst entrance for the  $10 \text{ l min}^{-1}$  than for  $5 \text{ l min}^{-1}$  case. For both cases, syngas formed partially in the oxidation zone as well as down stream. As expected, the increase in flow rate results in an increase in syngas production at the outlet. Relative amounts of  $\text{H}_2$  and  $\text{CO}$  formed in the presence of  $\text{O}_2$ , with respect to flow rate, do not vary significantly. The results do not exhibit significant  $\text{CO}_2$  reforming or water gas shift.

The modeling component of the investigation showed moderate qualitative agreement with experimental data, with the  $\text{C/O}$  ratio=1.0 exhibiting the most consistent agreement. One deviation of particular interest was the increase in the amount of water gas shift taking place observed in the theoretical model than in the empirical experiment at  $\text{C/O}=0.7$ . A large deviation in the model and the experiment was observed at the entrance but agreed better down stream. There were also deviations with the oxidation zone length, particularly with  $\text{C/O}=0.7$  and 1.3 (with the theoretical model) producing a zone 50% smaller than that produced in the empirical investigation. The authors postulate that the deviation in the  $\text{C/O}=0.7$  case is due to the mechanism not considering rhodium oxide. It is believed that more rapid methane activation than actually occurs during experimentation is predicted. In the  $\text{C/O} = 1.3$  case, the authors believe that carbon coverage may be more pronounced at the catalyst entrance than the model predicts, resulting in lower initial catalyst activity. No definitive conclusions are made with respect to these deviations.



This paper is understood to be the first published *in situ* investigation of partial oxidation of methane over rhodium. Though there are some key differences between the work produced by Horn et al. and the project presented in this thesis, the use of a rhodium catalyst to facilitate partial oxidation of methane accompanied with *in situ* diagnostics makes this article directly applicable to this research project. The use of a honeycomb monolithic catalyst versus the foam catalyst decreases the complexity of the impact from flow dynamics during operation. The parametric study presented in this thesis fixes C/O throughout the experiment and focuses solely on a larger range of space velocities in attempts to concretely confirm its impact on reformer operation. The ability to use this acquired data for analysis and design considerations is also demonstrated.

Kikas et al. [4], presents research that validates the hypothesis that reverse-flow (RF) reformers are more productive and effective than uni-directional (UD) reformers. This article boasts an increase of 5% in reaction selectivity towards H<sub>2</sub> and a 200°C decrease in the oxidation ignition temperature.

An optimal CH<sub>4</sub>/O<sub>2</sub> ratio between 0.7 and 0.8 was experimentally determined which resulted in H<sub>2</sub> selectivities between 70-80% and conversions between 55-60% for UD operation. RF reactors exhibited a 5% increase in selectivity and a conversion level comparable to that of UD operation. The improved thermal management that accompanies RF operation played a major role in the selectivity improvement. Flow reversal also decreased ignition temperature by 200°C and the RF and UD reactor skin temperatures remained low.

This paper offers preliminary empirical evidence that flow reversal improves reformer performance. This article speaks to the importance of thermal management in

these reformer systems, since it is the major contributing factor to the increase in reactor performance. The information presented in this work will be utilized in the discussion of the *in situ* temperature results in Chapter 4.

Kaissare et al. [12], presents a feasibility analysis of an operating RF and UD fuel reformer and presents an accompanying design. The work in this paper is an extension of the work presented in Kaissare et al.[10,11] discussed in Section 2.2. As with all UD and RF comparisons that have been presented, research shows that RF reformers are more productive than UD reformers. This work also claims that RF reformers are more capable of handling a wider array of changes in reaction parameters and that autothermal operation can only be maintained at higher H<sub>2</sub> throughput in RF reformers and not UD reformers.

The investigation presented in the paper studied the impact of feed ratio, switching time, catalyst loading and catalyst deactivation on operating reformers. All of the parametric studies exhibited the robust nature of RF operation. In addition, trends for both the UD and RF operations agreed with other literature and had similar impact on performance. Optimal switching time for RF operation was approximately 5 seconds and a set of optimal feed ratio values of 2:1 for UD operation and 1.16:1 for RF operation were realized.

Empirical evidence and parametric study results were presented that validated the use of RF reformers over UD reformers. The RF systems have been proven to be more productive in formation of H<sub>2</sub> and improve the thermal management of the systems. These findings also further support the general trends that have been presented in the literature for these reformers and a reliable system designs were also presented.

## 2.4 SpaciMS Literature

Partridge, et al. [14], speaks to the novel and useful nature of the SpaciMS system developed at Oak Ridge National Laboratories. *In situ* measurements are beneficial for numerous types of power and fuel reformation systems. The SpaciMS system is a tool that can acquire these measurements in a reliable and minimally invasive fashion. This article exhibits a demonstration of the very first internal diagnostic tool that is capable of acquiring internal transient measurements of an operating fuel cell in this manner.

Advanced-measurement-driven insights [14] are necessary in the investigation of fuel cells systems. A number of investigators have worked diligently to develop methodologies to obtain minimally invasive intra-reactor measurements. By blocking less than 3% of the flow-path and sampling at approximately  $10 \mu\text{L min}^{-1}$ , the SpaciMS system falls into this category.

Partridge et al. [14] explored the effect of load switching on PEMFC exhaust species concentration transients, conducted SOFC temperature fuel-cell effluent transient species measurements and measured intra fuel-cell species distribution measurements. Load switching had a distinct impact on species concentration within the fuel cell. Noticeable step changes were detected in  $\text{H}_2$ ,  $\text{O}_2$ ,  $\text{H}_2\text{O}$  and Ar with step changes in load. This component of the investigation did exhibit the negative effect that high water loading conditions could have on the capillary sampling system [Partridge, et al.]. High water loading could result in partial transient capillary occlusion or in worst case capillary clogging. For this reason, provisions were employed to ensure that intra-capillary condensation was mitigated.

The SOFC-temperature effluent (*i.e.*, *SOFC thermal conditions were replicated*) transient species measurements also exhibited a distinct step change in species with load changes. Starting with a load of  $200\Omega$ , decreasing to  $0.1\Omega$  and increasing back to  $200\Omega$ , hysteresis was observed. It is believed that this is due to the changing internal resistance of the fuel-cell. The high operating temperature of this experiment exposed the fragile nature of the capillaries at elevated temperatures. Once operating temperatures exceeded  $400^{\circ}\text{C}$ , the polyimide coating of the quartz capillaries burned off. This decreases the flexible nature of the capillaries, but if significant care is utilized, uncoated capillaries do not pose a significant reliability issue.

The intra-fuel-cell species distribution measurements used capillaries installed in the PEM fuel cell at  $0L$ ,  $0.15L$ ,  $0.46L$  and  $0.78L$  with  $L$  representing the serpentine path-length.  $\text{O}_2$  concentrations were measured along the path and load was varied. A gradual decrease in  $\text{O}_2$  concentration along the path length was observed with an increase occurring at the outlet. The author highlights this anomalous performance at the flow path outlet and attempts to attribute it to inter-cell and/or stack-level confounding issues.

This article offered a substantial background for understanding the novel and useful nature of the SpaciMS system. It exhibited the approach's capabilities in an operating fashion, demonstrating the capability to extract both transient and steady state measurements. The trends of the data agreed with operating-fuel cell fundamentals and offered some valuable insight into future scientific exploration. In conducting analysis with data acquired from this mechanism, it is necessary to confirm its validity as well as understand the complete and robust nature of the technology. This component of the literature search provided a background of understanding for the SpaciMS system.

## **2.5 Conclusion**

This literature review spoke to the three major components of this research project. The combination of empirical and computational investigations were reviewed in Sections 2.2 and 2.3, with Section 2.4 speaking to the novel SpaciMS instrumentation. A number of literature sources spoke to rhodium based partial oxidation catalysts, and the scope of the literature was broad, touching on thermodynamic analysis, RF/UD comparisons, C/O ratios parametric studies, and heat and mass transfer fundamentals. Both the empirical and computational components of the project are motivated and complemented by these citations.

## Chapter 3

### EXPERIMENTAL SET-UP

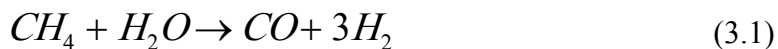
#### 3.1 SpaciMS Validation

The Spatially resolved capillary-inlet Mass Spectrometry system (SpaciMS), powered by a SRS RGA 100 quadrupole gas analyzer, is a mass spectrometer that employs the use of quartz, polyamine coated capillaries for sample gas mixture analysis. These capillaries have cross-sections on the order of micrometers (185 $\mu\text{m}$  outer diameter and 50 $\mu\text{m}$  inner diameter), which equips the SpaciMS with the capability to acquire *in situ* composition measurements of gas mixtures for various applications in a minimally invasive fashion. For this research project, the SpaciMS system is used to produce internal species composition profiles along the length of an operating CPOx reactor. The minimally invasive nature of the SpaciMS system is provided by the thin and malleable polyamine coated quartz SpaciMS capillaries. These capillaries are on the order of 50 $\mu\text{m}$  in inner diameter and 180 $\mu\text{m}$  in outer diameter. The reliability of the SpaciMS has been validated for a number of applications; but given the extreme nature of the thermal environment that was produced by the experiments conducted, verification of reliable results under extreme temperatures was essential to substantiating any findings and conclusions made from the SpaciMS data. A set of experiments, re-producing a more extreme version of the actual thermal environment than the SpaciMS capillary will experience during the study of an operating CPOx fuel reformer, was conducted to validate the results produced by the SpaciMS system.

### 3.1.1 Gas Phase Reaction Analysis

The operating reformer study consisted of experiments in which a fuel mixture of 27.6% CH<sub>4</sub> and 15.1% O<sub>2</sub>, balanced with Ar, was fed into a reactor, which contained a Rhodium-based, honeycomb monolith fuel reformer, to produce a mixture of CO and H<sub>2</sub>, also balanced with Ar. The reaction mechanisms proved to be complex, and there were three gas mixtures of particular interest that had potential to react, while in the gas phase, before arriving in the SpaciMS gas analyzer. The three gas mixtures of interest were the following: a.) 27.6% CH<sub>4</sub>, 15.1% O<sub>2</sub>, N<sub>2</sub>/Ar balance; b.) 34% H<sub>2</sub>, 17% CO, N<sub>2</sub>/Ar balance; c.) 13.8% CH<sub>4</sub>, 1.76% H<sub>2</sub>O, N<sub>2</sub>/Ar balance. Mixtures a and b are the inlet fuel and outlet product mixtures for the operating CPOx reformer experiment, balanced with an inert carrier gas. Mixture (c) is methane and water vapor balanced with an inert carrier gas. The concentrations for mixture (c) were arbitrarily selected to analyze the susceptibility to steam reformation. Mixtures (a) and (b) represent the inlet and expected outlet feeds for the operating reformer experiments respectively [4]. Mixture (a) concentrations were determined by experimental design and the concentrations of mixture (b) were determined by stoichiometry and prior art. Throughout the investigation, these mixtures will be sampled by the SpaciMS and be present in the gas phase during capillary transport. All three of these mixtures potentially pose a threat to intra-capillary gas phase reactions during transport. Confirming that these mixtures, in the presence of high temperatures, will not undergo a chemical reaction inside the capillary, before arriving in the gas analyzer, is thus imperative in validating the SpaciMS results. Prior investigations of catalytic partial oxidation broach the production of H<sub>2</sub>O as an intermediate product [4,7] throughout the reformation process and it is well known that

the highly endothermic steam reformation reaction exhibited in equation 3.1 can take place in high temperature environments.



Ensuring that this reaction was not occurring inside the capillary during transport was essential for validation of the instruments results. A set of experiments exposing a predetermined length of the capillary to a high temperature environment, feeding the capillary each of the mixtures of interest and analyzing the outlet with the SpaciMS were conducted. The compositions of all components of the mixture were plotted as a function of temperature and the errors in measurement associated with exposing each mixture to these extreme, high temperature environments were calculated.

#### 3.1.1.1 Experimental Set-Up

The Spatially Resolved Capillary-Inlet Mass Spectrometer (SpaciMS) was the main tool used to develop species profiles for the intra capillary gas phase reaction experiments. A 10 foot long capillary (50 $\mu$ m i.d., 185 $\mu$ m o.d.), connected to the SpaciMS Valco multiport valve was passed through a heated hose and inserted to the test rig that is illustrated in Figure 3.1. The SpaciMS capillary was threaded through a quartz tube (1.00 in o.d) that was fitted with a steel Swagelok end cap on each end. At the exit end of the quartz tube, the capillary was placed into a Swagelok fitting assembly through which the gas mixture of interest was flowed. The Swagelok fitting assembly was equipped with inlet and exhaust ports to assist with quick purging of the system. The capillary was secured in the Swagelok fitting with a nut and vespel ferrule assembly (ferrule: 200 $\mu$ m i.d.). The quartz tube was placed into a Lindburg/Blue M tube furnace. The capillary was threaded parallel to the length of the furnace which exposed the capillary to a heated zone



of 12 inches. With the furnace initially off, the gas mixture of interest was fed into the test rig and its composition was acquired using the SpaciMS system. Once that baseline measurement was taken, the furnace was heated to 700°C, the species profiles at the outlet were given time to stabilize, and the composition was measured. The furnace temperature was increased in 50°C increments and the outlet composition was measured until the furnace temperature was 1000°C. The outlet gas compositions were plotted as a function of temperature.

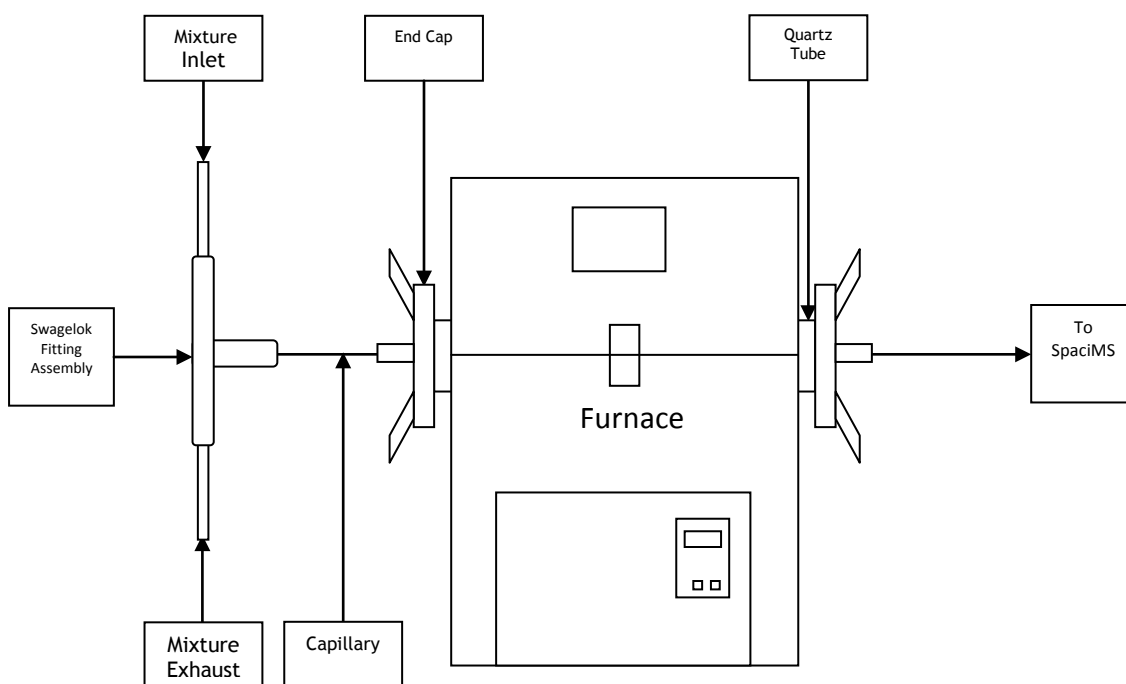


**Figure 3.1 : Intra-capillary gas phase reaction analysis experimental set-up for 12 inch heated zone**

An alternative test rig, illustrated in Figure 3.2, was assembled to conduct a similar set of SpaciMS validation experiments. This set of experiments utilized the same instrumentation excluding the quartz tube assembly. The capillary was fed through a slim opening on the hinge of the furnace and exited through the front face. The capillary was then inserted into the same Swagelok fitting, described in the initial set up, into which the

gas mixture of interest was fed. To protect the capillary from failure due to direct contact with the furnace brick, four pieces of insulating ceramic material less than 0.25cm thick were placed around the capillary, in between the furnace base and furnace top. In this set-up, the capillary was threaded perpendicular to the length of the furnace heater which exposed the capillary to a heated zone of 1.7035 linear inches but it is likely that the true hot zone spanned as much as 2 linear inches on each side of the furnace heater.

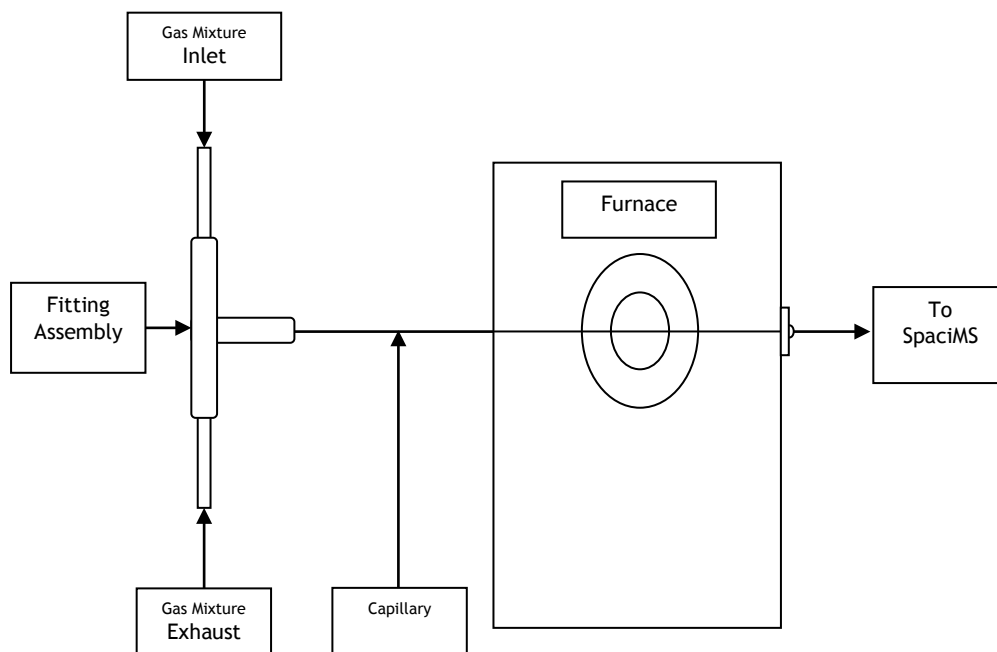


**Figure 3.2 : Intra-capillary gas phase reaction analysis set-up schematic for 1.7035 inch heated zone**

Each mixture was fed at 50 sccm and was facilitated by a mass flow controller (MKS Instruments, Inc.). Pressure changes using an Ion Gage and internal rig temperatures using an Omega type K thermocouple were recorded for each experiment.

### 3.1.1.2 Results

The Intra-capillary gas phase reaction analysis served as a reliability study of the SpaciMS system under operating conditions that would be experienced during the bench

flow reactor (BFR) reformer experiments. Understanding the chemical dynamics of the catalytic reactions that take place inside the reactor, a profile of expected species compositions were formulated. Given these gas mixtures of interest and high peak operating temperature of the catalyst, it was necessary to determine if reactions would occur during capillary transport from the reactor to the SpaciMS gas analyzer vacuum chamber.

For the purposes of determining the reliability of the SpaciMS for this particular set of experiments, three gas mixtures of interest were comprised and delivered to the test rigs illustrated in Figures 3.1 and 3.2 as outlined in section 3.1.1. The three mixtures of interest were: mixture (a.) 27.6% CH<sub>4</sub>, 15.1% O<sub>2</sub>, N<sub>2</sub> balance which is the actual initial fuel mixture (b.) 32% H<sub>2</sub>, 17% CO, N<sub>2</sub> balance, which is syn gas and the primary products of this reaction and; mixture (c.) 13.8% CH<sub>4</sub>, 1.76% H<sub>2</sub>O, N<sub>2</sub> balance, which is a mixture of the reactants of the steam reformation.

As previously stated, experiments were conducted exposing 12 in. and ≈6 in. (1.7035 + 2 in. on each side) of the capillary to an elevated temperature environment. The intra-*catalyst* peak temperature reaches approximately 1000°C over a 2 mm interval; therefore both the 12 in. and 6 in. hot zones are very extreme cases and we expect the temperature effects on the intra-*capillary* gas phase reactions to decrease with the decrease in heated length.

The SRS RGA 100 produces a signal that is dependent upon the number of species of a particular atomic mass unit (AMU) value that pass through the analyzer. Various species coincide with a number of different AMU values (N<sub>2</sub> corresponds to an

AMU value of 14 and 28)<sup>3</sup>, so the AMU values you decide to trace is dependent upon the composition of your gas stream. Two gas streams of differing but known composition are fed to the SpaciMS system and the signals produced are coupled with the known compositions to produce a calibration factor. This calibration factor is then multiplied by the signals acquired during the experiment to convert the signal provided by the gas analyzer, to an actual composition as illustrated in Equation 3.1.

$$CalFactor * Signal = Conc \quad (3.1)$$

Upon the conclusion of the intra-capillary gas phase reaction investigation, a statistical analysis was conducted on the SpaciMS system to determine the uncertainty of the measurements. Using the data from the 3 repeat experiments from mixture (a), a mean and standard deviation for both the signal values of species at room temperature and calibration factors were calculated. Once those values were acquired, Equations 3.2 - 3.4 were employed to determine the uncertainty of the species concentration values provided by the SpaciMS system

$$\Delta f = \sqrt{\sum_{i=1}^n \left( \frac{\partial f}{\partial x_i} \Delta x_i \right)^2} \quad (3.2)$$

$$\Delta x_i = 2\sigma \quad (3.3)$$

$$\Delta conc = \sqrt{(CalFactor * \Delta signal)^2 + (signal * \Delta CalFactor)^2} \quad (3.4)$$

Equation 3.2 is the general equation representing error propagation from measurement uncertainty. The measurement uncertainty for each component of the

---

<sup>3</sup> N<sub>2</sub> produced peaks at an AMU value of both 14 and 28 for the SGA gas analyzer. CO produces peaks at AMU values of 28 and 16. In order to delineate the 2 species during mass spectroscopy, a value of 14 should be used to quantify N<sub>2</sub> concentration and a value of 16 should be used to quantify CO concentration.

calculation is equal to twice its standard deviation as illustrated in Equation 3.3. Equation 3.4 represents the actual calculation of the concentration uncertainty.

The calculation was conducted for measurements of N<sub>2</sub>, CH<sub>4</sub>, and O<sub>2</sub>. The concentration uncertainty values attained were ± 4.401%, ± 2.807%, and ±0.598%, respectively.

The combustion of methane in the analysis of mixture (a) proved to be prevalent at elevated temperatures. As illustrated in Figure 3.3, when exposing the capillary to the full 12 linear inches heated region, noticeable O<sub>2</sub> and CH<sub>4</sub> depletion began to occur at 700°C; and at 900°C nearly all oxygen is consumed before the mixture reaches the vacuum chamber. An increase in N<sub>2</sub> concentration also occurs. CO<sub>2</sub> concentration also has a slight increase of approximately 1.2% at 1000°C. (note: CO<sub>2</sub> is graphed relative to the secondary axis on the right side of the graphic)

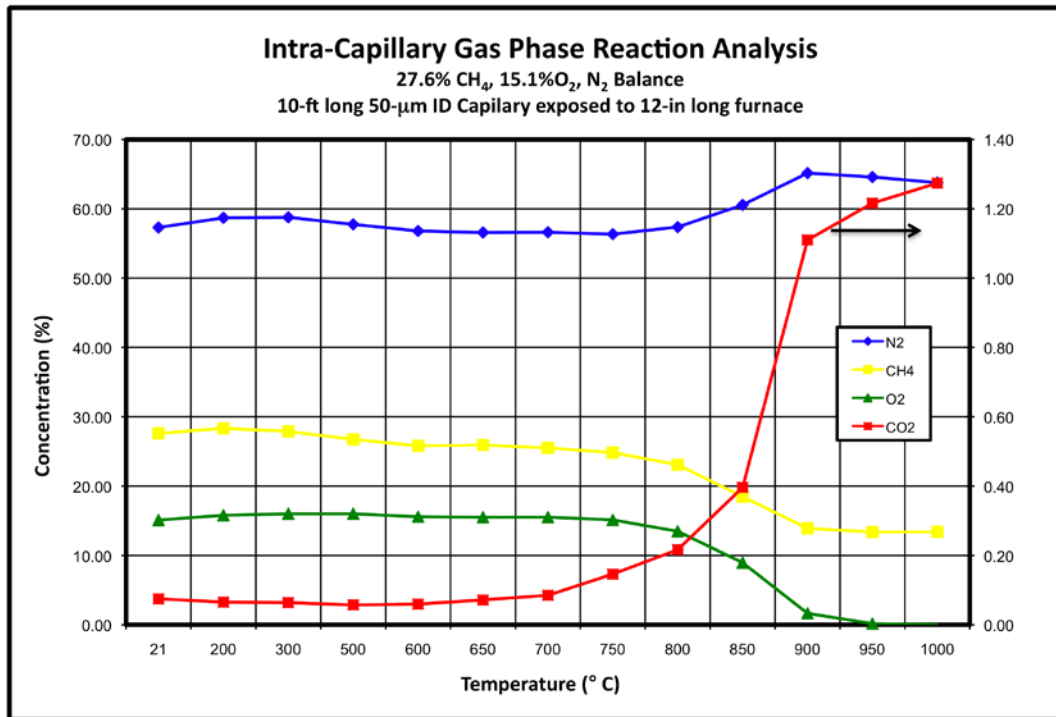


Figure 3.3 Intra-capillary gas phase reaction profile for inlet fuel mixture (a) as a function of temperature for the 12 inch heated zone

A similar experiment was conducted decreasing the heated zone of the capillary from 12 in. to 6 in. by using the experimental setup depicted in Figure 3.2. In this experiment an AMU value of 28 was used to track any changes with N<sub>2</sub> (which also coincides with CO and is illustrated on the figure). The width of the heated channel is actually 1.7035 inches but through inspection it appears that the actual heated zone extends two inches on each side of the channel, yielding a heated zone length of approximately 6 inches. For the experiments conducted in short channel test rig, the presence of a reaction is still evident but the decrease in the heated zone did yield favorable results.

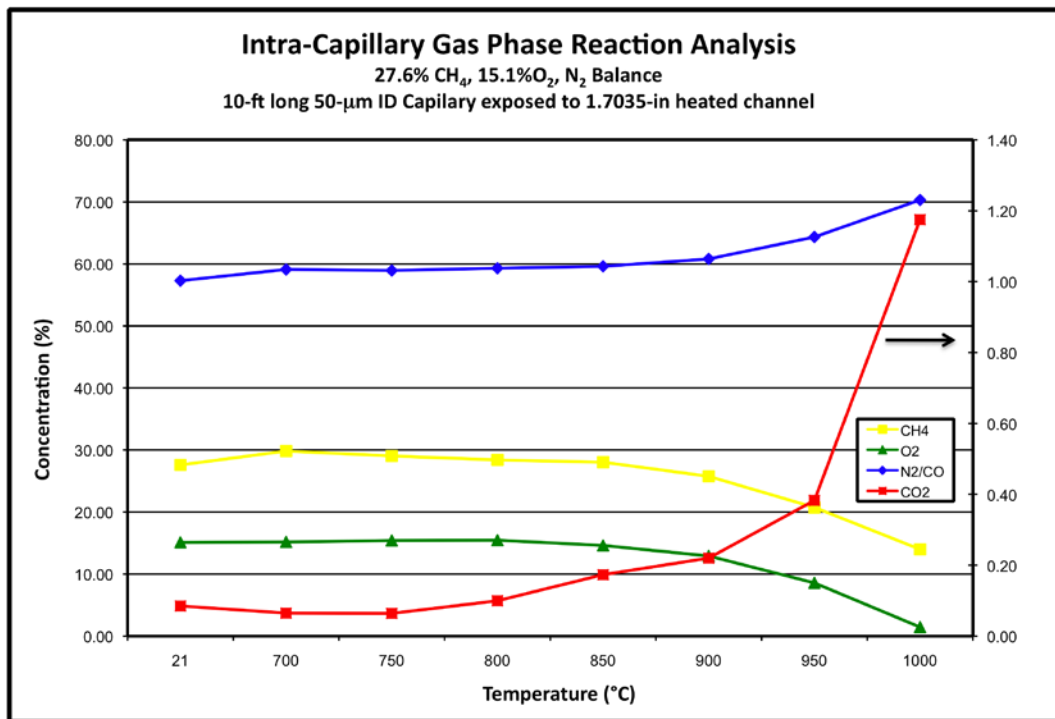


Figure 3.4 Intra Capillary gas phase reaction profile for inlet fuel mixture (a) as a function of temperature for the 1.7035 heated zone<sup>4</sup>

<sup>4</sup> N<sub>2</sub>/CO value denoted because an AMU value of 28 was used in the analysis

For the 6 in. case, illustrated in Figure 3.4, total consumption of O<sub>2</sub> occurred at 1000°C as opposed to 900°C in the 12 in. case. The slight formation of CO<sub>2</sub> occurred at higher temperatures but still increased by approximately 1%. Generally, significant intra-capillary reactions began to occur at higher temperatures and gas concentrations are less impacted by the temperature in the 6 in. heated zone experiment as compared to the 12 in. heated zone case. This appears to be due to the shorter length of the heated zone. Though these results exhibit a significant threat posed by mixture (a) for the occurrence of intra-capillary gas phase reactions, the decrease in CH<sub>4</sub> and O<sub>2</sub> consumption with the decreasing heated capillary length exhibits promise for validating the intra-*catalyst* SpaciMS measurements. The conclusion of the validation studies for mixture (a) are presented at the end of section 3.1.1.2.

Figure 3.5 is a graphical representation of the gas concentration profiles for mixture (b) fed into the test rig illustrated in Figure 3.1. As exhibited in the figure, the gas concentrations remain relatively constant with a slight decrease in H<sub>2</sub> and a slight increase in CO at higher temperatures. Each species has a concentration change of around 5%. Though this is not accounted for in the instruments level of uncertainty, recognizing that the 5% increase occurs at the most extreme thermal condition for a 12 in. heated zone, it is safe to conclude that under actual operating conditions (2-5 mm heated zone), that the impact of gas phase reactions would fall within the realm of instrument uncertainty.

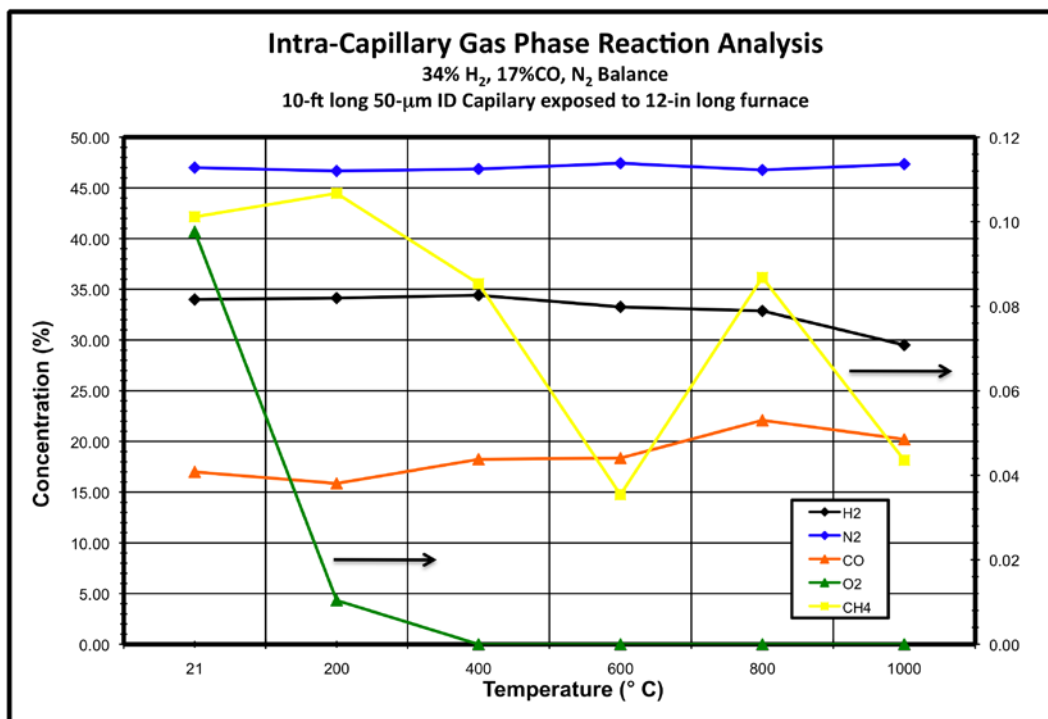
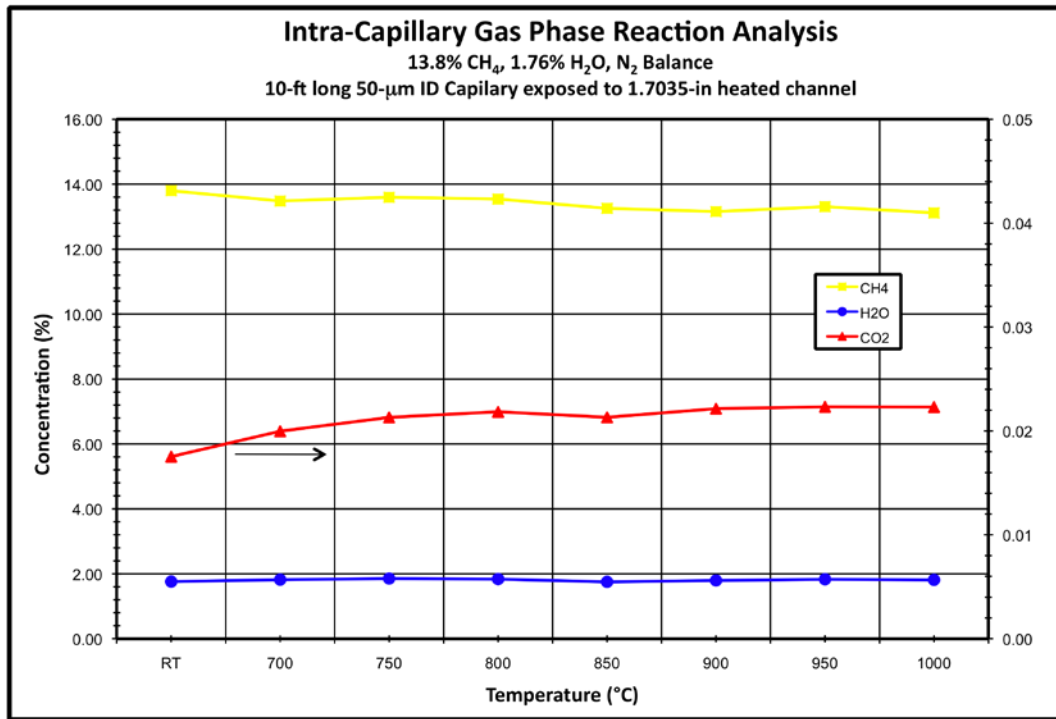


Figure 3.5 Intra-capillary gas phase reaction profile for outlet syn gas mixture (b) as a function of temperature for a 12 inch heated zone

Mixture (c) was used to analyze the likelihood of an intra-capillary steam reformation reaction occurring during transport to the vacuum chamber. Figure 3.6 illustrates a very slight decrease in methane concentration, less than 1%, accompanied by an even smaller increase in CO<sub>2</sub> concentration, less than 0.01% (note: that the CO<sub>2</sub> profile is presented with respect to the secondary axis on the right side of the plot). The “RT” on the temperature axis represents room temperature which was 21°C. The deviation in species concentration is well within the instrumental uncertainty of the SpaciMS system, and it is safe to conclude that no significant intra-capillary gas phase steam reformation is occurring during capillary transport.





**Figure 3.6 Intra-Capillary gas phase reaction profile for steam methane reforming mixture (c) as a function of temperature for a 1.7035 inch heated zone**

From the preliminary intra-capillary gas phase reaction experiments, the consumption of methane, the results of which are illustrated in Figures 3.3 and 3.4, posed the greatest threat for SpaciMS system to produce erroneous results. In attempts to confirm that the impact of reactions taking place in the SpaciMS capillary was negligible, the last set of gas phase reaction experiments, appropriately coined *intra-catalyst* gas phase reaction experiments, since the SpaciMS capillary is actually threaded through an operating catalyst, were designed to create an environment that could most accurately resemble that which the probe will encounter during actual reformer operation.

To produce this authentic operating environment, the SpaciMS probe was threaded through the actual operating bench flow reactor (BFR) assembly illustrated in Figure 3.7.

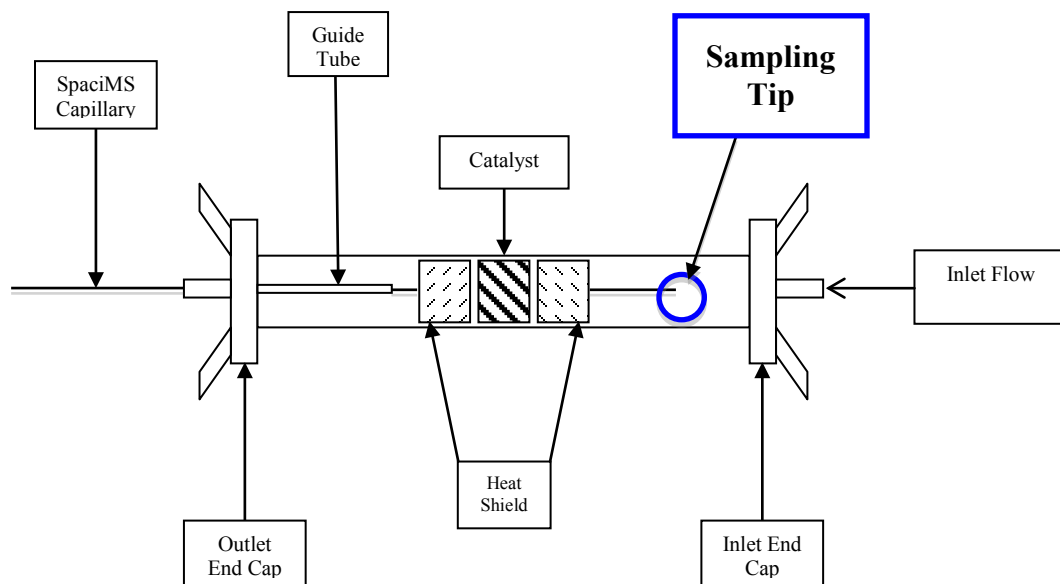



**Figure 3.7 Bench flow reactor quartz tube assembly - Intra-catalyst gas phase reaction analysis**

As will be explained in greater detail in section 3.3, the bench flow reactor assembly is placed in a furnace at 700°C and the fuel mixture of 27.6% methane and 15.1% oxygen, balanced with argon is fed into the reactor at a space velocity of 47 k hr<sup>-1</sup>. This space velocity produces the most extreme thermal environment (this is supported by data presented in chapter 4). This fuel mixture, fed into the reactor under these conditions results in reactor light off and the catalyst begins to facilitate the partial oxidation of methane resulting in a synthesis gas mixture exiting at the outlet. This mechanism of reactions is highly exothermic, thus much heat is released throughout the process and elevated temperatures result inside the channels of the honeycomb catalyst. For this experiment, a SpaciMS capillary was threaded from outlet to inlet of the BFR and the prescribed fuel mixture of 27.6% CH<sub>4</sub>, 15.1% O<sub>2</sub>, Ar balance was fed to the bench flow reactor at space velocity of approximately 47k hr<sup>-1</sup> to ignite the reformer and facilitate partial oxidation of methane. The end of the capillary was placed at the inlet of the BFR so that the inlet fuel mixture could be sampled. After passing through a portion of the

capillary that resided inside a channel of the operating reformer, that sample was analyzed by the SpaciMS system. The catalyst is 1-in in length and had a maximum, localized temperature of approximately 1300°C, for the 47k hr<sup>-1</sup> case, approximately 2 – 4 mm inside the entrance of the catalyst.

The results from the Intra-Catalyst gas phase reaction experiments are illustrated in Table 3.1. The concentrations of methane and oxygen are highlighted in green and yellow respectively. The results show that authentic operating conditions for the rhodium based partial oxidation fuel reformer of interest do not result in intra-capillary chemical reactions in the gas phase. The methane and oxygen concentrations for the operating reformer scenario are elevated, which is actually evidence of no reaction since the two species would be consumed through oxidation, but the CH<sub>4</sub> value varies by 1.62%, which is well within the prescribed accuracy of the system. The results also show no increase in the concentration by products that result from combustion or partial oxidation of methane, thus further affirming the fact that no significant chemical reactions take place intra-capillary in the gas phase and the SpaciMS produces reliable data.

**Table 3.1. Intra-Catalyst gas phase reaction results**

<b>Intra-Catalyst Gas Phase Reaction: Concentrations (%)</b>						
	<b>H2</b>	<b>CH4</b>	<b>Ar</b>	<b>CO</b>	<b>O2</b>	<b>CO2</b>
<b>Dormant</b> FT=21°C <b>Reformer</b> <b>Off</b>	0.06	27.32	61.02	0.07	15.52	0.04
<b>Operating</b> FT=700°C <b>Reformer</b> <b>On</b>	0.05	28.94	64.03	0.05	15.91	0.03

There are 2 independent variables that play a role in the rate and existence of intra-capillary gas phase reactions, temperature and exposed capillary length. Though temperature inside the operating reformer can exceed 1000°C for some flow conditions, the length of capillary that is actually exposed to the most extreme of the thermal conditions is small. For the small capillary length in a high temperature environment, the effects of these independent variables compete, but the analysis illustrated in table 3.1 shows that the impact of intra-capillary gas phase reactions on system accuracy for a capillary exposed to the thermal environment created by the operating fuel reformer is negligible.

### **3.2 Instrumentation Development**

The primary mission of this research project was to prove that the instrumentation developed in house at ORNL (i.e. SpaciMS) could reliably and accurately acquire *in situ* data of an operating CPOx fuel reformer as well as improve the spatial resolution of said measurements. Prior to conducting this research project, preliminary experiments were conducted with the SpaciMS system on both operating fuel reformers and fuel cells, but the spatial resolution was very low and the experiments were conducted in a coarse fashion. To improve the accuracy and reliability of the experiments as well as streamline the process as a whole, data acquisition processing changes were made to the pre-existing test rig before this new set of experiments began. The first was the construction of the translation stage. The translation stage is an apparatus that is used to translate the temperature and SpaciMS probes along the length of the reactor with high spatial resolution and accuracy. The second was automation of data acquisition through the use of National Instrument's LabView software. A virtual instrument was developed in house

to quickly and accurately acquire temperature and position data. The use of the translation stages coupled with the operating capabilities of the Lab View software greatly improved the accuracy and reliability of the experimental results.

### **3.2.1 Translation Stage**

The translation stages were constructed and added to the experimental set-up to ensure accurate spatial resolution when acquiring the desired *in situ* measurements. The core component of the translation stage was a Vexta 2 phase DC stepping motor (Model number PX245-01AA) operated by a Velmex VMX stepping motor controller. The stepping motor was affixed to the MA-150 uni-glide system and moved the translation platform with an accuracy of 1/400<sup>th</sup> of a millimeter. The Velmex stepping motor controller was connected to a Dell Inspiron 8200 laptop computer via RS232 interface and was controlled using a virtual instrument created with National Instruments Lab View Software. The virtual instrument (VI) design allowed the input of a desired translation distance, in millimeters, along with a direction. The VI also included the capability to automate an entire acquisition process by inputting the number of translations along with the length of the translations, in millimeters, and the motor would translate along the uni-glide track until all steps of the desired length were taken.

#### 3.2.1.1 Thermocouple Stage

Figure 3.8 illustrates the translation stage used to propel the thermocouple along the length of the BFR. The thermocouple used is an Omega engineered type K thermocouple ( Part# KMTSS-010E-24). The thermocouple is 24 inches in length and 0.25 millimeter in diameter. The temperature was extracted from the thermocouple using a National Instruments Hi-Speed USB Carrier (Model Number NI USB-9162),

accompanied with a National Instruments LabVIEW virtual instrument interface that was developed in house.

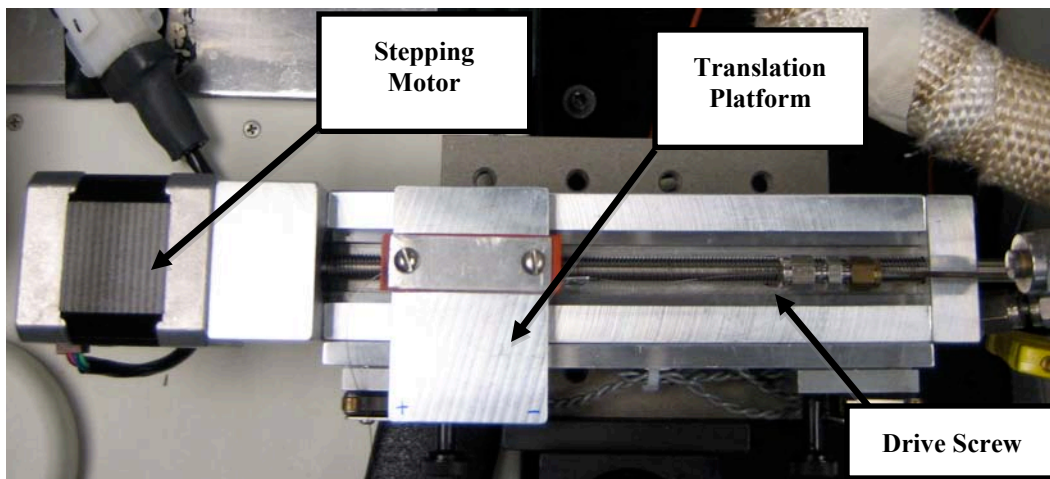


**Figure 3.8 Thermocouple translation stage**

The translation platform consists of a flat aluminum plate with two rectangular pieces of rubber (orange) and a rectangular aluminum cover affixed to its surface. The thermocouple was placed in between the two pieces of rubber and secured to the translation platform by tightening the screws illustrated in Figure 3.8. The translation platform was connected to the drive screw, which was powered by the vexta stepping motor, all illustrated in Figure 3.8. The drive screw has a spatial resolution that is proportional to the angle of rotation. This drive screw translates the platform 1 mm per rotation and the smallest rotation that the motor can provide is  $1.8^\circ$ , thus resulting in a maximum spatial resolution of  $1/200^{\text{th}}$  of a mm.

The acquisition of the temperature data utilized the automated acquisition method described earlier in this section. The thermocouple was translated along the length of the operating reactor and both heat shields (see Figure 3.7) in 0.2 mm steps. From this data, temperature plots, illustrating the stream temperature as a function of linear position along the length of the reactor, were generated and presented in Chapter 4.

### 3.2.1.2 SpaciMS Capillary Stage

The same attribute that make the SpaciMS capillaries such a valuable investigative tool (i.e. their small size that makes them so minimally invasive for *in situ* measurements), also makes them fragile, delicate, and for this particular application, susceptible to intra-capillary condensation. It is for this reason that the SpaciMS capillary translation stage required a more complex design than that for the thermocouple.

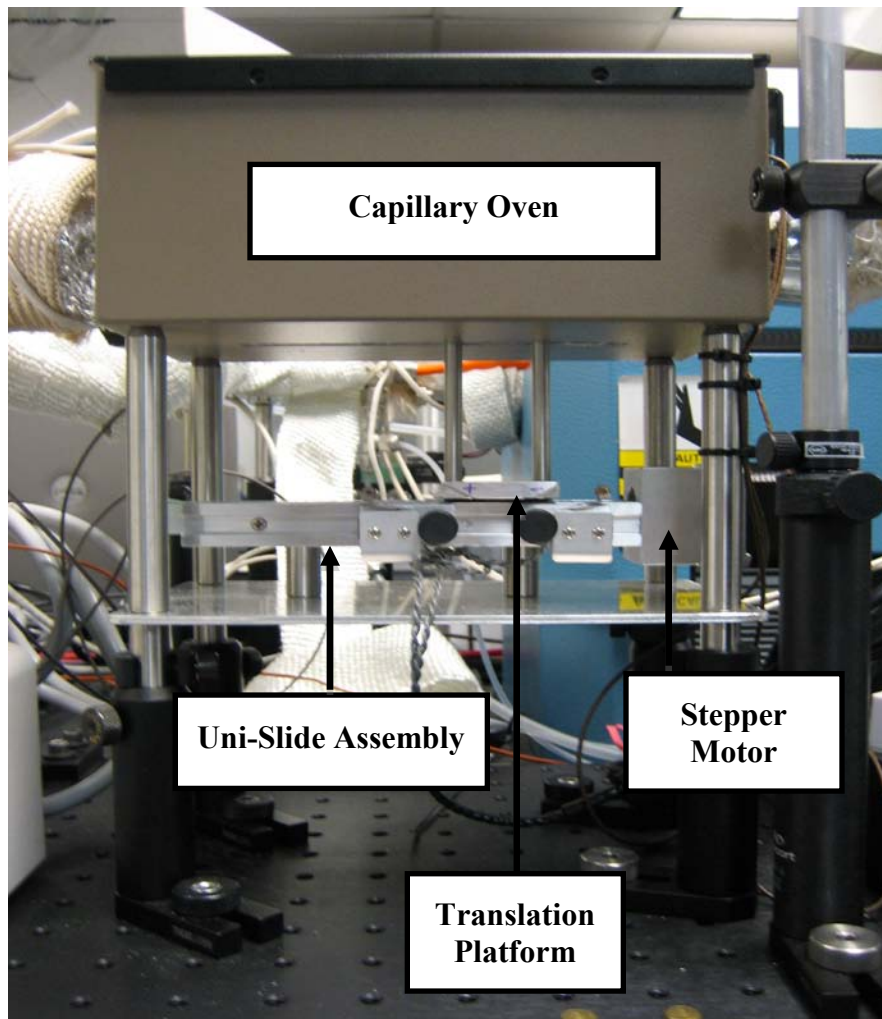


Figure 3.9 SpaciMS capillary translation stage

Figure 3.9 illustrates the SpaciMS capillary translation stage. As indicated in the picture, the translation mechanism for the SpaciMS stage is the same as for the thermocouple stage. The identical uni-slide assembly, stepper motor and translation platform comprise the translation mechanism. Figure 3.9, however, shows two aluminum rods extending from the translation platform into the capillary oven. Affixed to those two rods, inside the capillary oven are two flat pieces of aluminum with two pieces of flat rubber affixed in between the aluminum plates, mimicking the thermocouple assembly presented in section 3.2.1.1, the SpaciMS probe is secured by placing it in between the flat rubber sheets

Due to the capillary's susceptibility to internal condensation, the capillary must be insulated and heated along its entire length. The capillary is enclosed in insulation and heat tape along its entire length, but the complex geometry of the translation stage is what requires the need for the capillary oven. The heat tape, operating at a temperature of approximately 150°C is used to prevent condensation of H<sub>2</sub>O in the capillary. Figure 3.3 illustrates, that for the 12 in. of exposed capillary case (worse case scenario) that intra-capillary reactions are not present until the 700°C temperature threshold is reached, thus, the heat tape poses minimal threat to the production of accurate SpaciMS measurements. The capillary oven is a steel box lined with an insulating material, and a heat source is housed inside to combat the internal condensation. There is a narrow channel in the bottom of the oven that allows for the aluminum rods to translate.

Preliminary experimentation exhibited the presence of a "reaction zone" near the entrance of catalyst. The majority of the chemical reactions that take place in the reformer occur within this zone. The SpaciMS probe was translated by the same Virtual



Instrument used to translate the thermocouple and the data was acquired using a software package that accompanies the gas analyzer. The SpaciMS data points takes longer to acquire (sampling rate =  $10\mu\text{L min}^{-1}$ ) than the temperature data, thus a variable spatial resolution was employed. A resolution of 1 mm was used through the inlet heat shield, then a 0.2 mm resolution was used throughout the reaction zone, gradually being increased to 0.4 mm down the length of the reactor eventually arriving at 2.0 mm at the reactors exit and in the outlet heat shield. Species profiles as a function of position and space velocity will be presented in Chapter 4.

### 3.3 Bench Flow Reactor Set-Up

The bench flow reactor is the test rig that was used to characterize the operating fuel reformer using the minimally invasive, *in situ* measurement mechanism provided by the SpaciMS. Figure 3.10 illustrates the quartz tube assembly of the bench flow reactor.

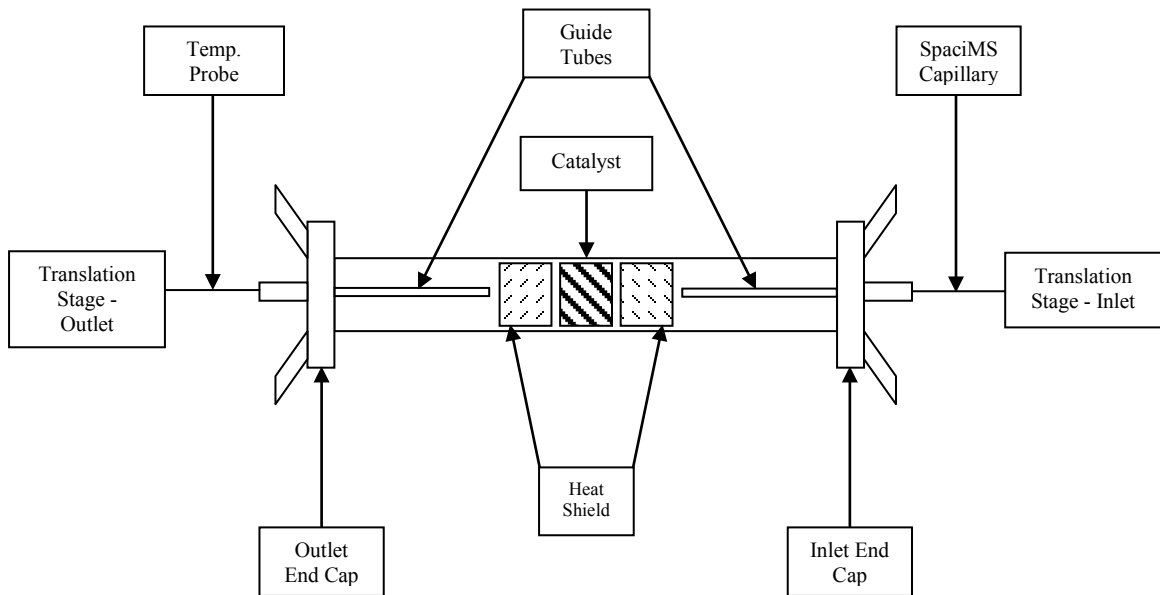


Figure 3.10 Bench flow reactor quartz tube assembly

The rhodium-based catalyst (0.8 in. o.d., 1.00 in. long) resides in the center of a quartz tube (1.00 in. o.d.). The catalyst was wrapped in a ceramic based insulating material to limit heat loss in the radial direction and insure a snug fit in the quartz tube. A honeycomb substrate, wrapped in the ceramic insulating material to serve as a heat shield, was placed on each side of the catalyst with approximately a 2 mm separation gap. The quartz tube was sealed with Swagelok end caps through which a guide tube was threaded on each side. The guide tubes were placed approximately 15 mm from the exterior faces of the heat shields. The guide tubes were included in the assembly of the test rig to assist with the insertion of temperature probes and sampling capillaries. The quartz tube was then placed in a Lindberg/Blue M furnace, illustrated in Figures 3.1 and 3.2, and heated to 700°C.

The inlet side of the test rig is where the fuel mixture is introduced. A mixture of 27.6% CH<sub>4</sub> and 15.1% O<sub>2</sub> balanced with Ar was sent into the reformer. As illustrated in Figure 3.1, the SpaciMS capillary is attached to, and moved by the inlet translation stage, which is described in detail in section 3.2.1.2 and inserted through the guide tube. The capillary was placed 8 mm deep into the outlet heat shield and extracted until it was 8 mm deep into the inlet heat shield. Initially the capillary is moved in 2 mm increments but spatial resolution is increased, ultimately to 0.2 mm increments, as the capillary approaches the catalyst inlet.

The outlet side is where the exhaust port is positioned. All species that are final products of the reformer reactions exit the rig through the outlet and are delivered to an FTIR Spectrometer for analysis. Delivered to the test rig, through the outlet, is an Omega

type K thermocouple. Similar to the SpaciMS capillary, the thermocouple is affixed to the translation stage to ensure accurate spatial resolution.

The fuel mixture of 27.6% CH<sub>4</sub> and 15.1% O<sub>2</sub> balanced with Argon was used throughout the experiment. The quartz tube assembly was placed into the furnace and the furnace was ramped up to 700°C, and the entire assembly was allowed to arrive at thermal equilibrium with the furnace. Once thermal equilibrium was reached, and the temperature and SpaciMS probes were in place, the fuel mixture was fed into the BFR. The mixture was allowed to flow for approximately one hour, until the system heated up and reached steady state. Once at steady state, temperature and species measurements were acquired. This process was conducted at space velocities of 47k hr<sup>-1</sup>, 75k hr<sup>-1</sup>, 100k hr<sup>-1</sup>, 150k hr<sup>-1</sup>.

## CHAPTER 4

### EXPERIMENTAL RESULTS DISCUSSION

#### 4.1 Temperature Analysis Results

The temperature acquisition mechanism described in section 3.2.1.1 was designed to capture *in situ* temperature measurements of an operating fuel reformer. Section 3.3 illustrates the bench flow reactor (BFR) set up and outlines the procedures in the experimental process. As previously listed, the temperature measurements are acquired using an Omega type K thermocouple. The thermocouple used was a special limits of error thermocouple, as stipulated by the National Institute of Standards and Technology (NIST) and has an instrument uncertainty of  $\pm 2^\circ\text{F}$  (i.e.  $\pm 1.11^\circ\text{C}$ ) or 0.4% of the actual reading, what ever is higher [15]. For the sake of the majority of the temperature data acquired, the latter applies.

The BFR quartz tube assembly is heated to a temperature of  $700^\circ\text{C}$  in a tube furnace and a fuel mixture of 27.6%  $\text{CH}_4$  and 15.1%  $\text{O}_2$  balanced with Argon is fed to the bench flow reactor at space velocities of  $47 \text{ k hr}^{-1}$ ,  $75 \text{ k hr}^{-1}$ ,  $100 \text{ k hr}^{-1}$ ,  $150 \text{ k hr}^{-1}$ . Once the system reaches steady state and the furnace temperature stabilizes, *in situ* temperature measurements were taken along the length of the reformer catalyst and both heat shields in 0.2 mm increments. SpaciMS species measurements were acquired at a variable spatial resolution, with finer resolutions being employed throughout and in regions adjacent to the reaction zone. This data was collected for all four space velocities of interest. Figure 4.1 illustrates a plot of stream temperature as a function of position for all four space velocities.

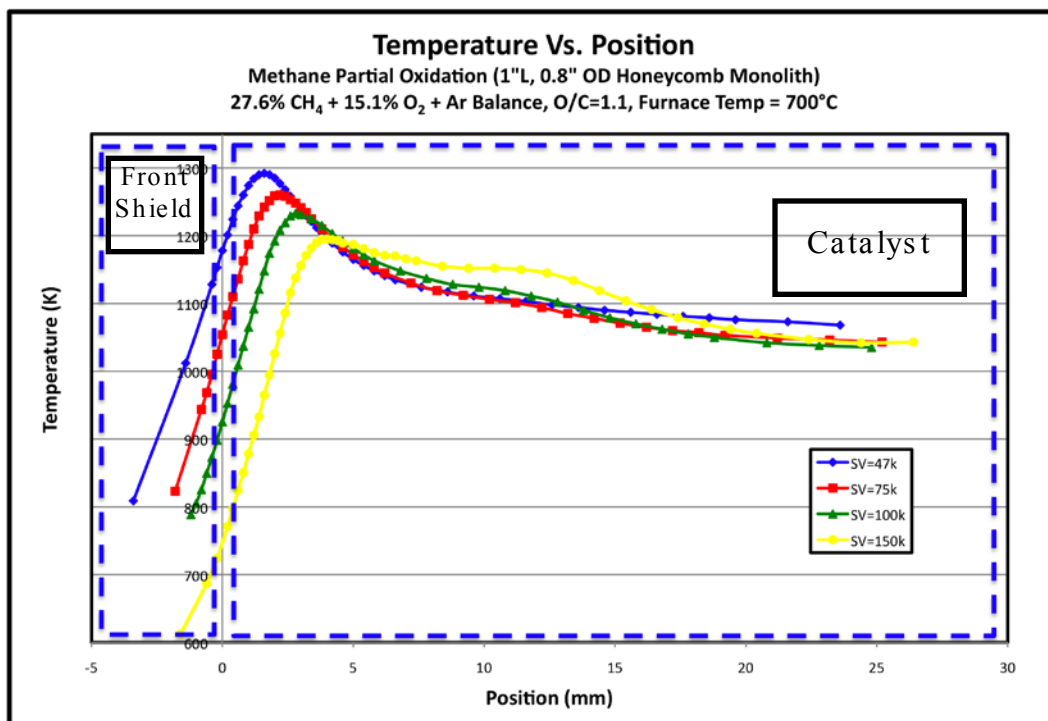


**Figure 4.1 Temperature vs. Position as a function of space velocity**  
(Note: Units of space velocity are hr<sup>-1</sup>)

The flow of fuel mixture with respect to Figure 4.1 is from left to right (i.e. fuel is flowing through the front shield, through the catalyst, and out of the back shield which is not illustrated in the figure). The temperature of the fuel entering the BFR was not controlled, so the inlet temperature at the face of the catalyst varies with space velocity. Assuming that all constituents left the cylinders at approximately the same temperature, the decrease in inlet fuel temperature at the face of the catalyst with increased space velocity is expected since its residence time in the furnace is lower and the feed has less time to obtain heat from the operating furnace. The heat capacitance rate of the feedstock is higher with increased flow rate and at higher space velocities as well, thus resulting in less temperature increase. The fuel mixture is fed into the front heat shield and eventually reaches some maximum temperature well within the first 5 mm of the catalyst. Again, a trend in the location of the peak temperatures as a function of space velocity is exhibited.

As space velocity increases, the location of the peak temperature along the length of the catalyst increases.

Table 4.1 displays the inlet catalyst temperature, the peak temperature and peak temperature location for all four space velocities.

**Table 4.1 Peak temperature location for given space velocities**

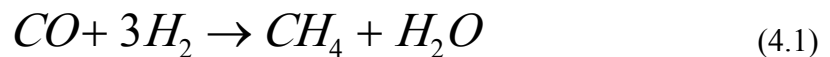
<b>Space Velocity</b>	<b>Inlet Catalyst Temperature</b>	<b>Peak Temperature</b>	<b>Peak Temperature Location</b>
<b>[hr<sup>-1</sup>]</b>	<b>[K]</b>	<b>[K]</b>	<b>[mm]</b>
47k	1178	1292	1.6
75k	1054	1260	2.2
100k	925.1	1233	2.8
150k	745.7	1195	3.8

For the low space velocity case of 47 k hr<sup>-1</sup>, the peak temperature occurs 1.6 mm into the face of the catalyst whereas for the 150 k hr<sup>-1</sup> case, the peak temperature location occurs at 3.8 mm into the face of the catalyst. The rhodium-based catalyst is a millisecond contact time reformer. At higher space velocities, the catalyst is exposed to more fuel mixture hence, more active sites are required to facilitate the desired reaction. This implies that more active sites downstream are occupied and a greater number of reactions are taking place on a longer portion of the catalyst length, thus the location of the peak temperature is expected to shift downstream.

Prior art [3] and SpaciMS data substantiate the presence of a “reaction” zone within the first 5mm of the catalyst for all space velocities. The reaction zone is the area of the catalyst where majority of the chemical reactions, that constitute partial oxidation, take place. These chemical reactions are highly exothermic and the primary cause for the presence of these peak temperatures in this region of the reformer.

Not controlling the feed inlet temperature at the face of the catalyst poses the potential impact of confounding effects and presents a disadvantage in arriving at some strict and definitive conclusions on the impact of space velocity on the temperature profile along the length of the reactor. Accordingly, a decrease in peak stream temperature and an increase in peak temperature location with increasing space velocity is observed; however, the fact that the independent inlet temperature variable was not controlled challenges the appropriateness of definitively resolving the reasons for those trends. With that stated, it is expected, that the decreased stream temperature at the catalyst inlet can have a cooling effect on the over-all stream temperature profile, thus decreasing peak temperature; additionally, the increased space velocity has an increased heat capacity rate thus also altering the temperature profile.

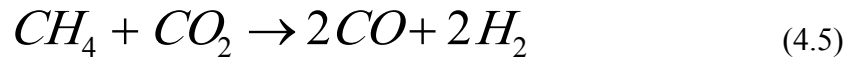
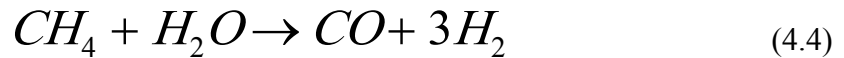
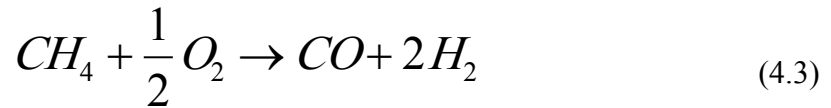
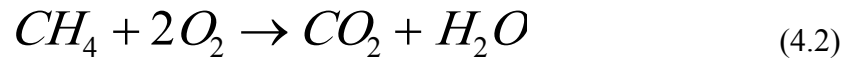
As space velocity increases, an inflection in the temperature profile down stream is observed, this is indicative of the presence of the methanation reaction occurring down stream. The methanation reaction is actually the reverse of the steam reformation reaction and is highly exothermic. It is illustrated below in Equation 4.1.



As alluded to earlier in this section the fundamental function of a catalyst is to decrease the necessary activation energy for a reaction of interest. From inspection of the temperature profile and supporting evidence from the SpaciMS profiles in section 4.2, the combination of significant stream temperatures, large enough CO and H<sub>2</sub> concentrations and the presence of the rhodium based catalyst create an environment that could promote the occurrence of this reaction.

## 4.2 SpaciMS Results

The four chemical reactions of interest that comprise the prevalent methane reaction mechanisms are presented below in Equations 4.2 – 4.5. Equations 4.2 - 4.5 represent the combustion, partial oxidation, steam reformation and dry reformation reactions respectively.



These 4 reactions illustrate 6 constituents that could possibly be present in the reactor at any given time. Inclusion of argon or nitrogen, as a balance carrier gas, into that list yields a total of 7 species that must be tracked by the SpaciMS system throughout the investigation. As with the temperature experiments, measurements were taken along the length of the reactor as well as both heat shields. The temperature measurements had a spatial resolution that was uniform along the length of the reactor. Given the more involved and time consuming process of acquiring SpaciMS measurements, a variable spatial resolution was employed during data acquisition, which included decreasing down



to a step size of 0.2 mm in the proximity of and throughout the reaction zone.

Measurements were taken in 2 mm steps through the beginning of the inlet heat shield, eventually decreasing the resolution to 1 mm and arriving at 0.2 mm upon entering the face of the catalyst. Data was acquired through the reaction zone (up to approx 4 mm into the catalyst) at a spatial resolution of 0.2 mm, increasing to 0.4 mm at the exit of the reaction zone then increased to 1 mm from approximately 6 mm into the catalyst to 20 mm into the catalyst. Measurements were acquired in 2 mm steps through the exit of the catalyst and the inlet heat shield. The SpaciMS probe was held at each measurement location for 30 seconds. This was sufficient time for the sample to travel to the gas analyzer and for the GUI interface to update and exhibit a stabilized species composition. Species profiles along the length of the catalyst and the heat shields were taken for all 4 space velocities of interest.

Figure 4.2 illustrates the composition of all 7 species of interest as a function of position for the  $75 \text{ k hr}^{-1}$  space velocity experiment. All concentrations are calculated on a molar basis (i.e. mole fraction). Similar plots were generated for the other three space velocity cases. In attempts to remain consistent with the temperature plot, fuel flows from left to right with respect to this graph. As the plot illustrates, a fuel mixture of 27.6%  $\text{CH}_4$ , 15.1%  $\text{O}_2$ , balanced with what equates to 57.3% Ar is fed into the face of the inlet heat shield, which is represented by -10 mm on the position axis. 0 on the position axis represents the entrance of the catalyst. As is evident from the figure, the fuel composition begins to change between 2 mm and 3 mm into the catalyst, which signifies the start of a chemical reaction and is consistent with the peak temperature location that is presented in Table 4.1.

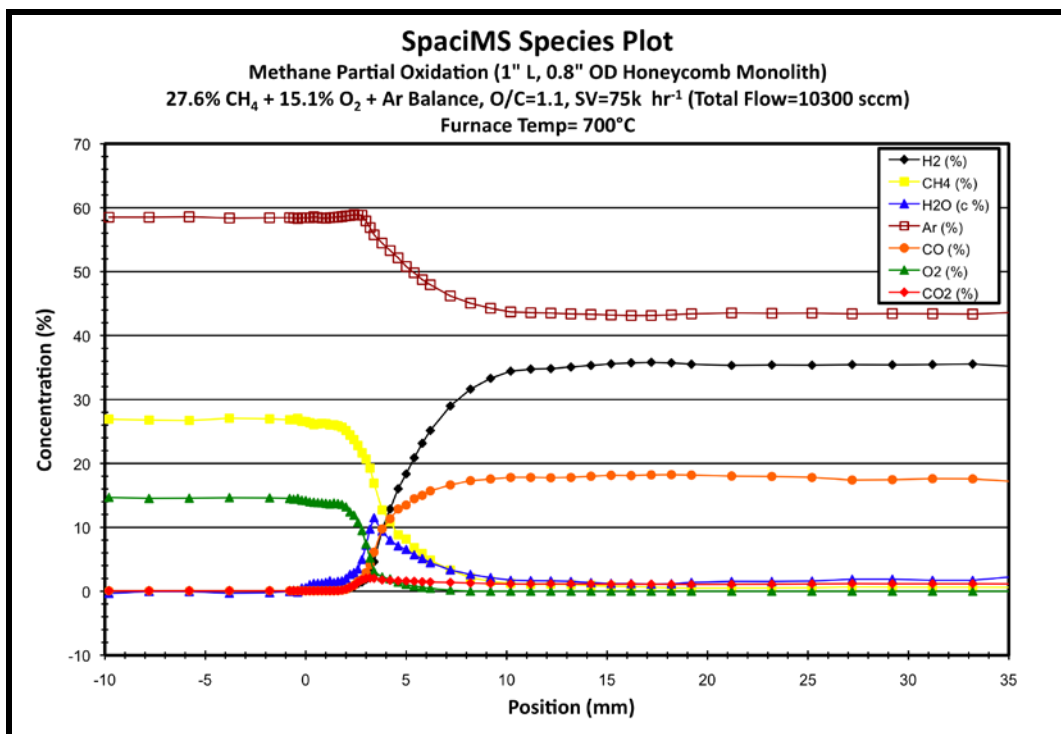


**Figure 4.2 Species composition as a function of position for 75k hr<sup>-1</sup> experiment**

Once chemical reactions begin to take place inside the reactor, we see an immediate decrease of methane and oxygen, and products delineated in Equations 4.2-4.5 begin to form. Water is produced at the onset of the chemical reactions. The plot shows a peak value of just below 10% composition of H<sub>2</sub>O between 3 mm and 4 mm into the catalyst followed by immediate consumption. The near complete depletion of oxygen, aligns with the concentrations of CH<sub>4</sub> and H<sub>2</sub>O becoming equal and CH<sub>4</sub> approaching the zero concentration baseline at approximately the same trajectory. This is consistent with the 1 to 1 CH<sub>4</sub> : H<sub>2</sub>O ratio that is exhibited in the steam reformation reaction illustrated in Equation 4.4. This substantiates the presence of the steam reformation reaction. CO<sub>2</sub> concentration shows a maximum value between 3 mm and 4 mm along the catalyst, but its value never appears to pass a concentration of 2% and once reaching its maximum value, the concentration quickly baselines to a 0% concentration. This consumption of

CO<sub>2</sub> in the presence of an excess of methane supports the existence of the dry reformation reaction illustrated in Equation 4.5. The composition at the outlet is 35.4% H<sub>2</sub>, 17.8% CO with a balance of Ar with all other species baselined at low compositions close to 0%.

Figure 4.3 illustrates the species composition as a function of position along the length of the reformer for the 150 k hr<sup>-1</sup> experiment. Similar to the 75 k hr<sup>-1</sup> plot, the inlet composition illustrated at the entrance of the inlet heat shield is consistent with the stated fuel feed composition. Continuing down the x-axis, we observe the onset of chemical reactions taking place between 4 mm and 5 mm down the length of the catalyst, which is consistent with the length of the reaction zone presented in Table 4.1. The portion of the plot that illustrates the composition at the outlet of the catalyst and heat shields shows a composition comparable to that of the synthesis gas produced in the 75 k hr<sup>-1</sup> case and all other species approach and arrive at low single digit percentage composition baseline. A notable difference between Figure 4.2 and 4.3 is the CH<sub>4</sub> concentration between the reaction point and the end of the catalyst as well as the noticeable inflection points in the H<sub>2</sub> and CO plots. In the 75k hr<sup>-1</sup> case, the methane and water vapor concentrations reached the same value approximately 2 mm outside of the reaction zone and approached the base line at the same trajectory. In the 150 k hr<sup>-1</sup> case, both methane and oxygen approach the baseline at a similar trajectory, but they do not begin to follow that same path until approximately 5 mm down stream from the reaction point and their values do not become equal until they both are at their baseline exit concentrations. Upon inspection, inflection points are also present in the H<sub>2</sub> and CO plots. This coupled with the elevated methane concentration values and the slight inflection in the methane plot

around the 15 mm mark, substantiate the presence of the methanation reaction at higher space velocities, as broached in Section 4.1. The slight decrease in the rate of hydrogen and carbon monoxide production and increase in the rate of methane and water vapor production, are consistent with the methanation reaction presented in Equation 4.1 and substantiates the presence of this “reverse” reformation. SpaciMS species plots for the remaining space velocities are presented in Appendix C.

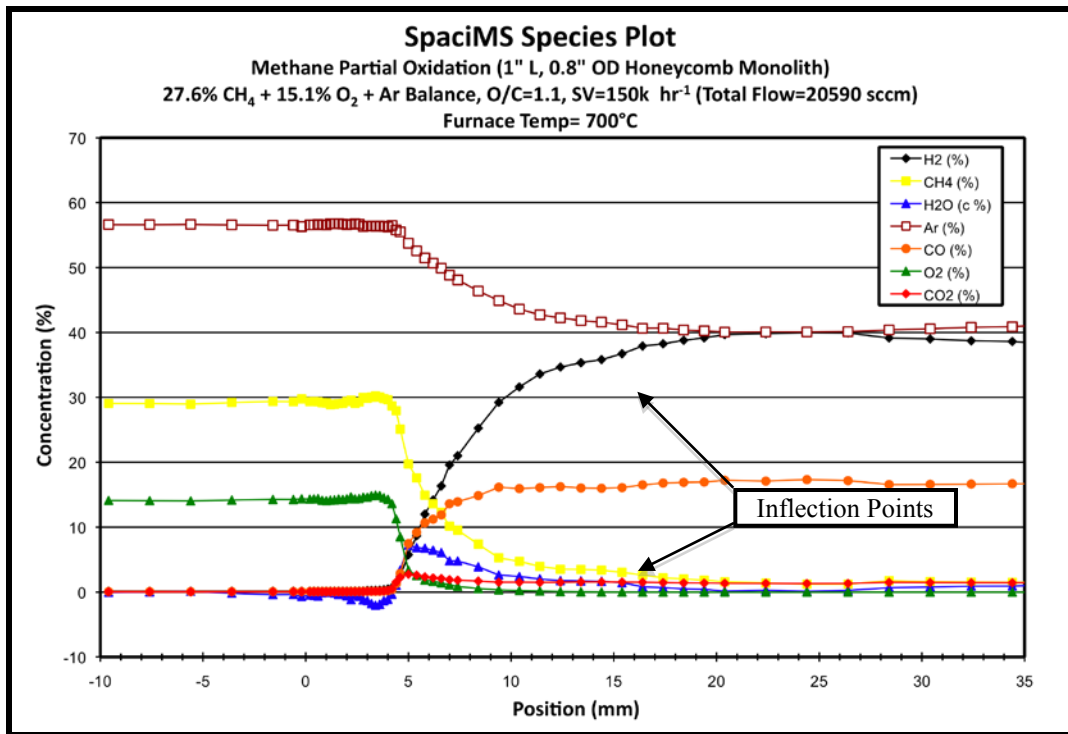
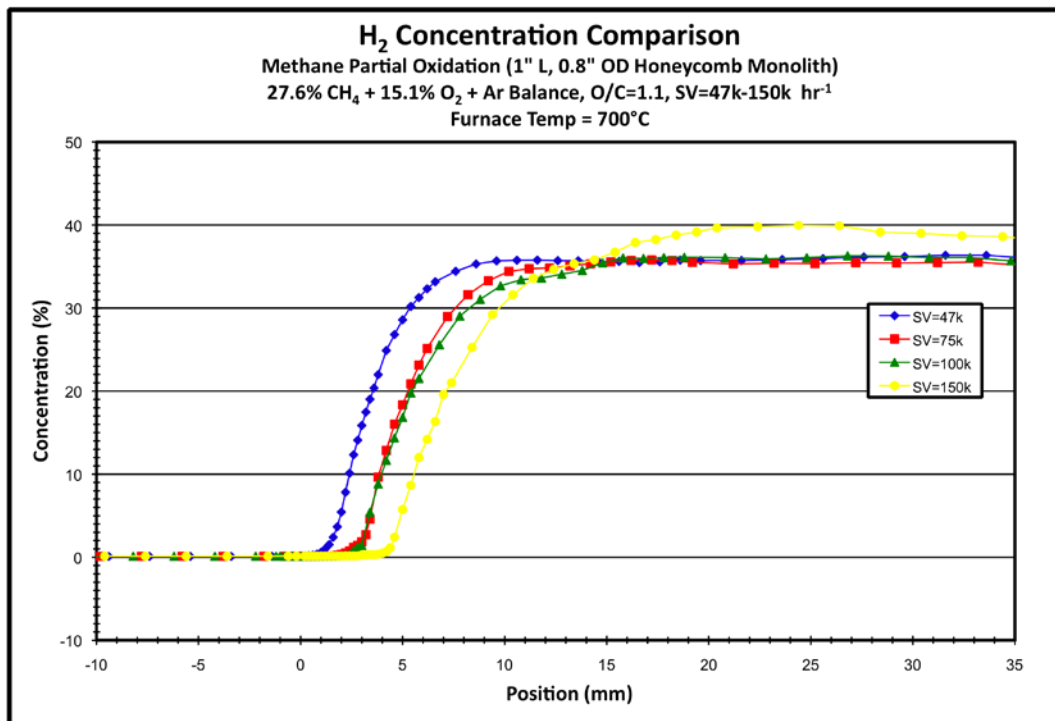


Figure 4.3 Species composition as a function of position for 150k hr<sup>-1</sup> experiment

Figure 4.4, which presents the concentration of hydrogen as a function of position for all four space velocities of interest, illustrates the presence of this inflection and increase in reaction point and reaction zone length. Upon inspection, the most evident observation is the linear placement, along the x-axis, of the point where the concentration curves begin to approach their outlet value. Generally, as space velocity increases, the location where a zero slope is attained after the upward turn in the concentration curve is

translated further along on the x axis with the 47 k hr<sup>-1</sup> case beginning its upturn between 2 mm and 3 mm and the 150k hr<sup>-1</sup> case beginning its upturn between 4 mm and 5 mm. The more pronounced presence of these inflection points is more evident in Figure 4.4. For the 47k hr<sup>-1</sup> case, the upturn and plateau is smooth with no noticeable inflections in the curves shape. As space velocities increase, especially for the 100k hr<sup>-1</sup> and 150k hr<sup>-1</sup> cases, the presence of this inflection point, between 10 mm and 15 mm down the catalyst length, which supports the presence of the methanation reaction, is more prevalent.



**Figure 4.4 Hydrogen concentration as a function of position across all space velocities (Note: Units of space velocity are hr<sup>-1</sup>)**

Figure 4.5, the same type of plot as Figure 4.4 with methane as the gas of interest, provides another piece of evidence for the same argument but from the other side of the

chemical equation. Concentration comparison plots for other species of interest are presented in Appendix C

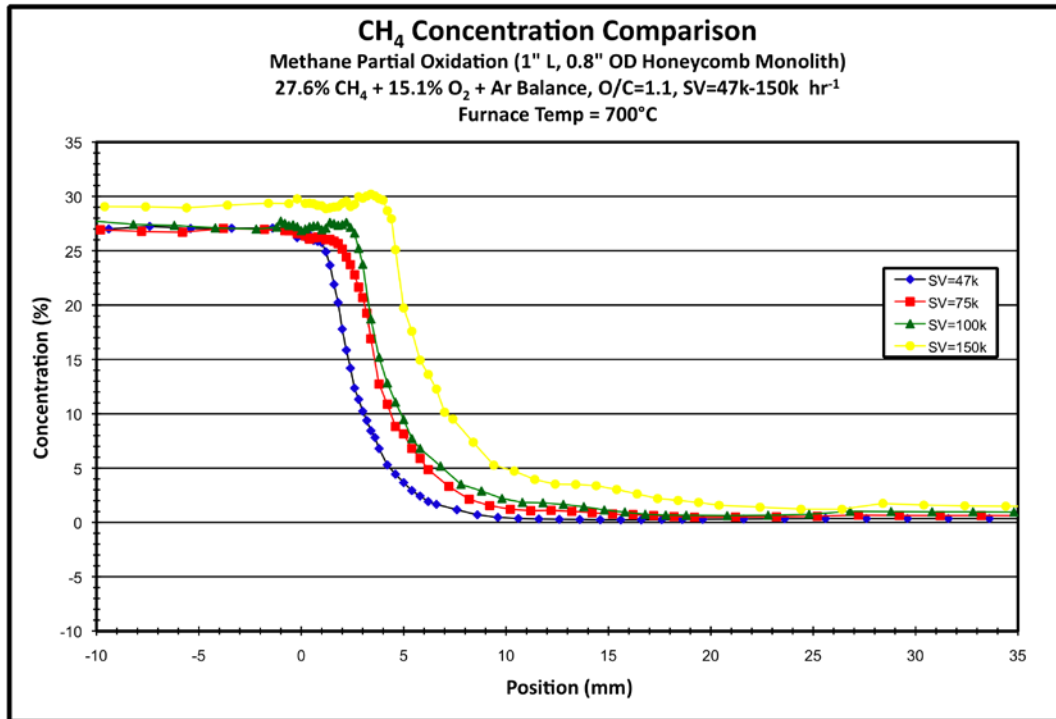


Figure 4.5 Methane concentration as a function of position across all space velocities (Note: Units of space velocity are hr<sup>-1</sup>)

# CHAPTER 5

## COMPUTATIONAL MODEL DEVELOPMENT

### 5.1 Qualitative Analysis

#### 5.1.1 Engineering Equation Solver Justification

The ability to acquire *in situ* spatial measurements of an operating thermal system component is a very powerful investigative tool; furthermore, novelty resides in utilization of these measurements to conduct thermodynamic analyses. An analysis tool was developed using Engineering Equation Solver (EES) to characterize the operating fuel reformer on a thermodynamic basis utilizing the *in situ* measurements acquired by both the SpaciMS and temperature acquisition mechanisms. Standardized flow rate and inlet composition are system parameters measured prior to the start of each experiment and internal temperature and composition measurements are extracted from the reformer during operation, via the method outlined in Chapter 4. As stated in Chapters 3 and 4, improved spatial resolution was a major focus for this research project so, converting this large amount of raw data extracted from the temperature and SpaciMS diagnostic systems, as well as the standardized operating parameters, to a useable form can prove to be computationally intensive with respect to volume and complexity. Throughout the experiment, high quantities of data (40-50 data points per axial station for each experiment) are extracted along the length of the reactor. A system or method that could decrease the computational intensity of this project is essential.

Given the computational intensity of the required analysis, the large amount of data that needed to be manipulated, and the well-defined analysis methodology, EES was a viable platform for this analysis. EES is an iterative solver that can successfully solve

systems of equations consisting of over 25000 variables. EES syntax is simplistic, relative to most programming languages, and in addition to ease of use, it has a vast thermophysical property database that streamlines the process of obtaining necessary property values and calculating parameters of interest. EES is also equipped with various features such as solution tables and formatted equations windows, which makes the data easily transferable to Microsoft Excel for analysis and provides easy-to-read equation sheets presented in a comprehensible form.

### **5.1.2 EES Code Development Methodology**

EES Code was designed to conduct thermodynamic analysis of the operating fuel reformer using in situ data obtained from the SpaciMS and temperature measurements systems. Prior art [3,5] exhibits that for a millisecond contact time reformer of this nature, catalytic partial oxidation starts within the first 5 mm of entering the reactor. The region within the reactor, where the majority of the chemical reactions are taking place is known as the reaction zone and the initial point and length of the reaction zone have been shown to be directly correlated with the space velocity of the feed stock. For this reason, the experiments were designed to employ a finer measurement resolution (0.2 mm) throughout, and in the proximity of, the reaction zone and to employ a coarser resolution (0.4 mm and 1.0 mm) outside of the reaction zone.

This data acquisition method segments the reactor into slices, each of which can be treated like its own independent, one inlet – one exit, open thermodynamic system. The lengths of these slices varies from as small as 0.2 mm to 1 mm, depending on spatial resolution used at that portion of the reactor. All of the slices have the same cross-sectional area proportional to the 0.8 in. outer diameter of the honeycomb monolith.



In Figure 5.1, the rhodium-based honeycomb monolith catalyst used in the reactor is illustrated. This design, which consists of channels with a very small hydrodynamic diameter, ensures laminar flow through the catalyst and increases surface area which results in efficient and reliable contact with the noble metal based catalyst. Though the monolith does occupy some volume, for the sake of the computational analysis conducted for this project, we will presume plug flow [5].

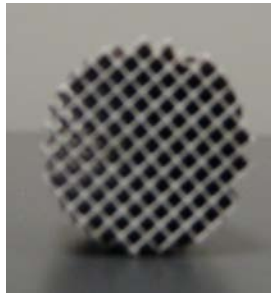


**Figure 5.1 CPOx honeycomb monolith catalyst – cross sectional view**

While the experiment was being conducted, the system was allowed to reach equilibrium before data was acquired. The monitoring temperature displayed by the furnace remained relatively constant, decreasing at a rate of approximately  $3^{\circ}\text{C/hr}$ , and minimal mass was accumulated inside the reactor (minor coking on the catalyst after extended operation). These experimental conditions substantiated the applicability of a steady state assumption for conducting thermodynamic analysis. Given there was no work output, and that there were negligible changes in both kinetic and potential energy, a simplified version of the equation governing the first law of thermodynamics of an open system was formulated as presented in Equation 5.2.

$$\dot{Q}_{released} = \sum_n (\dot{m}_n h_n)_{in} - \sum_n (\dot{m}_n h_n)_{out} \quad (5.2)$$

The subscript  $n$  on the summation symbols represents the number of inputs and outputs, into and out of the open system respectively. As employed in the code, this equation simultaneously accounts for changes in temperature and composition. The  $\dot{m}$  terms represent the mass flow rate of the respective species and  $h$  is the specific enthalpy of the species entering or exiting the system.  $\dot{Q}_{released}$  represents the amount of heat released due to the chemical reaction within the slice of the reactor of interest. This heat released is expected to correspond with an increase in stream temperature.

The EES code was developed to thermodynamically analyze the operating reactor along its entire length. Using the virtual reformer “slices” or volumes, that were created by the measurement methodology, the written code, treats each slice like an independent thermodynamic system and analyzes each slice as such. The discrete point at which data is acquired along the reactor length, as illustrated in Figure 5.2, determines the inlet and outlet of each slice. Using acquired data, a thermodynamic assessment of the operating reformer system can be obtained.

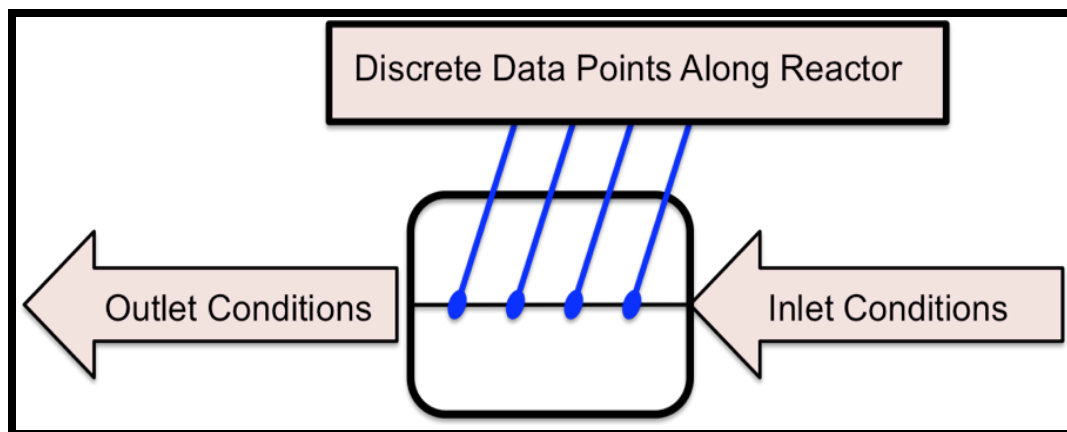


**Figure 5.2: Data acquisition discretization schematic**

The operating conditions for each experiment is detailed by space velocity, furnace temperature and inlet composition. The foundational responsibility of the code was to transform this data that resulted from the operating conditions of the reactor for each experiment into a form that could be more easily utilized. The first task was converting the standardized volumetric flow rate that coincided with each space velocity into both molar and mass flow rates. Table 5.1 displays the four space velocities for the four different experiments along with their corresponding standardized volumetric flow rates. The standardized volumetric flow rate quantifies the volume of gas that would be flowing if it were at standard temperature and pressure ( $T = 298\text{K}$ ,  $P = 1\text{atm}$ ,  $\mu = \text{molar mass of inlet mixture}$ ).

**Table 5.1: Space velocity with corresponding standardized volumetric flow rates**

<b>Space Velocity</b>	<b>Standardized Volumetric Flow Rate</b>
<b>[hr<sup>-1</sup>]</b>	<b>[sccm]</b>
47k	6500
75k	10300
100k	13730
150k	20590

In order to determine the actual molar and mass flow rates, this standardized volumetric flow rate had to be converted to an actual volumetric flow rate. This actual volumetric flow rate, which is variable along the reactor, in conjunction with variable temperatures and compositions are tracked and integrated into the subsequent calculations. The equation used, which was derived from the ideal gas equation of state, is displayed below in Equation 5.3. “P” represents the pressure, “T” represents the reactor temperature and “ $\mu$ ” represents the molar mass of the mixture at a given data acquisition point. It is also important to note, that because there is a change in composition along the length of the reactor, it is necessary to include a molar mass correction factor in the conversion equation ( $\mu_{std}$  = molar mass of inlet fuel mixture). Once the actual volumetric flow rate has been resolved, the ideal gas law is again employed to determine the actual molar flow rate. That conversion is displayed in Equation 5.4. “P”, again, represents the pressure inside the reactor, “R” represents the universal gas constant on a molar basis and “T” represents the stream temperature.

$$\dot{V}_{actual} = \dot{V}_{std} \times \left( \frac{\mu_{std}}{\mu_{actual}} \times \frac{T_{actual}}{T_{std}} \times \frac{P_{std}}{P_{actual}} \right) \quad (5.3)$$

$$\dot{n}_{actual} = \frac{P \dot{V}_{actual}}{RT} \quad (5.4)$$

The molar flow rate is converted into individual mass flow rates of each species in Equation 5.5. In this equation,  $x_n$  represents the mole fraction of a given species,  $\dot{n}_{actual}$  is the actual molar flow rate resolved in Equation 5.4 and  $\mu_n$  is the molar mass of the particular species of interest.

$$\dot{m}_n = X_n \dot{n}_{actual} \mu_n \quad (5.5)$$

Total mass flow throughout the reactor can be quantified by summing up all of the individual species mass flow rates at each slice. To confirm that our steady state assumption held, total mass flow rate was calculated and found to be consistent through each slice for all 4 cases. Table 5.2 illustrates the mass flow rates for each of the 4 space velocities.

**Table 5.2: Space velocity with corresponding mass flow rates**

<b>Space Velocity</b>	<b>Total Mass Flow Rate</b>
<b>[hr-1]</b>	<b>[g/s]</b>
47k	0.155
75k	0.247
100k	0.329
150k	0.493

Once the mass flow rate was resolved, the first law thermodynamic analysis could be conducted. The energy balance equation that was employed is displayed in Equation 5.2. This equation takes the mass flow rate of each species and multiplies it with the specific enthalpy of each species at the respective temperature, and those values are summed at the inlet and outlet of each slice. The value that results is the heat released for that slice from the reaction mechanism that is carried out in the presence of the rhodium-based catalyst. The result from this analysis will be discussed in Section 5.2. Due to a lack of sufficient operating data being available, second law analyses were not conducted. The code, however, has the capability to conduct this analysis given the appropriate system operating data (i.e. an appropriate boundary temperature profile for entropy analysis).

## 5.2 Quantitative Analysis

### 5.2.1 1<sup>st</sup> Law Analysis

Figure 5.3 illustrates the Heat vs. Position plot, normalized by mass flow of fuel. As expected, for all cases, a large spike in the  $\dot{Q}$  value is observed within the reaction zone. The “bursts” in heat released values occur further away from the entrance of the reactor with increasing space velocity, with the 100k  $\text{hr}^{-1}$  space velocity data varying from this trend. Intuitively, relatively constant normalized maximum heat released values are expected across the regime of space velocities. The maximum normalized  $\dot{Q}$  values for 47k  $\text{hr}^{-1}$  and 75k  $\text{hr}^{-1}$  are approximately equal, yet the max value for the 100k  $\text{hr}^{-1}$  case is greater than the max value for the 150k  $\text{hr}^{-1}$ .

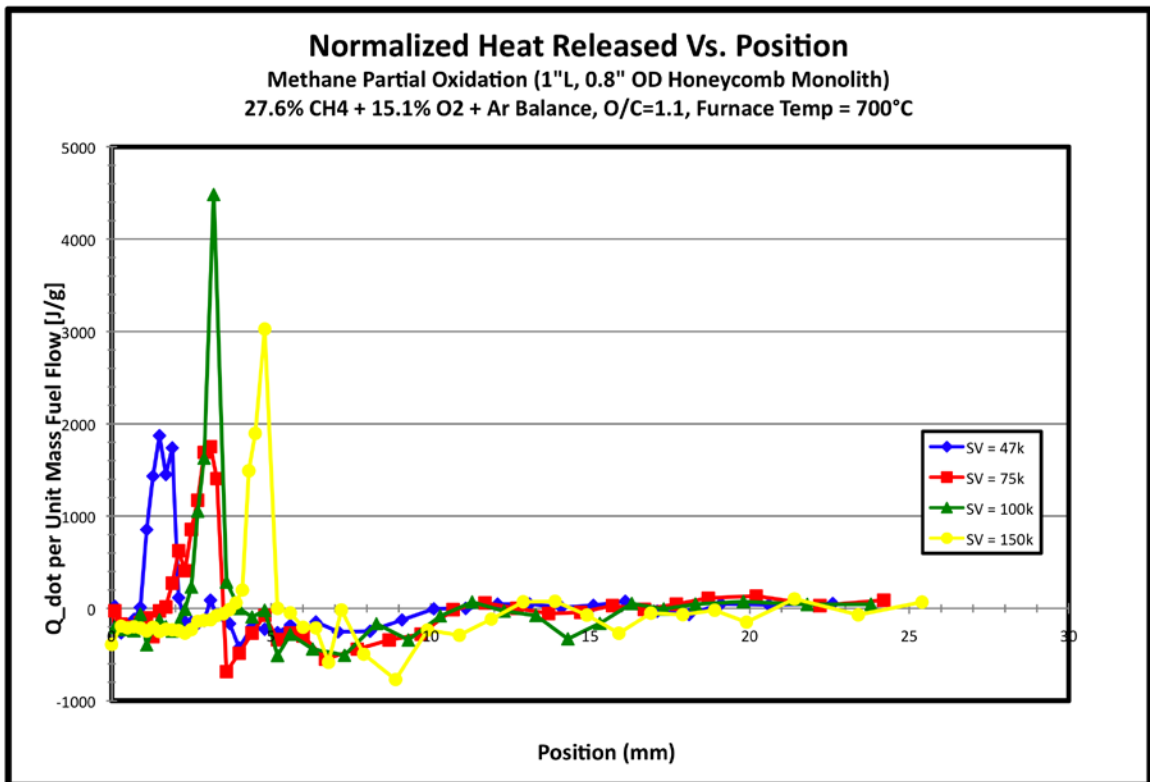


Figure 5.3 : Heat Released Vs. Position normalized by fuel flow

The downstream axial translation of the heat released peaks as space velocity increased was consistent with both the temperature and species profile data presented in Chapter 4. At increased space velocities (i.e. increased flow rates) the advective displacement is expected to increase, resulting in feed occupying active sites further downstream. This is manifested in the shifting of the heat released peaks exhibited in Figure 5.3. The increase in peak heat released values for both the 100k hr<sup>-1</sup> and the 150k hr<sup>-1</sup> cases, as presented in Figure 5.3, are however deviations from the expected result. Having normalized the heat released values with the respective mass flow for each case, a more uniform magnitude for peak height across all space velocities was expected and not observed. With regard to the 150k hr<sup>-1</sup> case, Figure 4.5 shows that there was a slightly increased concentration of CH<sub>4</sub> than in the other 3 test cases. This increase in fuel could potentially substantiate the increase in peak normalized heat released value observed. Upon further investigation and discussion, no physics based evidence supporting the magnitude of the peak heat released value for the 100k hr<sup>-1</sup> case can be provided and is believed to be the result of experimental or computational error. Low cylinder pressure, SpaciMS capillary translation error, issues with the discretization scheme or an error in calibration procedures are all viable sources of potential experimental or computational error.

The analysis presented in Figure 5.3 is the product of single experiments conducted at each space velocity of interest. This project, though intended to provide scientific insights, was primarily focused on developing the instrumentation to characterize reformers in an in situ fashion as well as validating and exhibiting its capability. From an experimental perspective, replicates of these experiments at each

space velocity need to be produced and analyzed from both a physical and statistical standpoint. A comprehensive and well-conducted investigation of that nature will allow us to better characterize with a high level of reliability the internal operation of this fuel reformer.



# CHAPTER 6

## CONCLUSION

### 6.1 Summary of Results

A system that could extract internal data from an operating CPOx fuel reformer was constructed. *In situ* temperature and species data of an operating rhodium based partial oxidation fuel reformer was acquired and used to conduct thermodynamic analysis. The outcomes of this project provide evidence that reliable, *in situ* diagnostics can be acquired from operating fuel processors and that acquired data can be used to produce useful analysis for insight into component and system development.

Primarily, an intra-capillary gas phase reaction validation analysis for the SpaciMS (Spatially resolved capillary Mass Spectroscopy) system was completed. The goal of this study was to confirm that the results produced by the SpaciMS during the BFR experiments were accurate; more specifically, to confirm that sampled mixture did not undergo reactions in the gas phase while in transit from the capillary sampling tip to the gas analyzer. Three gas mixtures of interest were identified for this verification exercise: mixture (a.) 27.6% CH<sub>4</sub>, 15.1% O<sub>2</sub>, N<sub>2</sub> balance; mixture (b.) 32% H<sub>2</sub>, 17% CO, N<sub>2</sub> balance; mixture (c.) 13.8% CH<sub>4</sub>, 1.76% H<sub>2</sub>O, N<sub>2</sub> balance.

Preliminary experimentation, allowed two of the gas mixtures to be eliminated from this list. The one mixture that reacted in the gas phase in an extreme thermal environment was the Bench Flow Reactor (BFR) inlet fuel mixture of 27.6% CH<sub>4</sub>, 15.1% O<sub>2</sub> balanced with the non-reactive N<sub>2</sub>. A follow-up experiment, which involved decreasing the exposed length of the capillary, from 12 in to 2 mm, was conducted. For the 2 mm case, which represents the approximate length of the reaction zone where the

thermal environment is most extreme, minimal conversion was observed and the results fell well within the accuracy of the system. The reliability of the SpaciMS, under the extreme thermal conditions that are presented by this experiment, was validated.

BFR experiments were subsequently conducted and analyzed. The BFR is an intricate experimental system, which includes the translation stages for both the SpaciMS and temperature probes, along with the catalyst assembly and preheat tube furnace. Design and construction of these instruments was integral to producing reliable data that would allow definitive and substantive conclusions to be made. Oak Ridge National Laboratory (ORNL) facilitated the development of this complete diagnostic system, with the SpaciMS data verification and increased spatial resolution through probe translation serving as the areas of specific contribution from this thesis project. The improved spatial resolution of both the temperature and species measurements provided the opportunity to characterize the reformer along its axial length and provided reliable spatial data for computational analysis. The experiments conducted supplied the same fuel mixture of 27.6% CH<sub>4</sub> and 15.1% O<sub>2</sub> balanced with the non-reactive Ar gas, at space velocities of 47k hr<sup>-1</sup>, 75k hr<sup>-1</sup>, 100k hr<sup>-1</sup>, 150k hr<sup>-1</sup>. The results from the experiments showed a general trend of an increased maximum temperature with decreasing space velocity as well as an increased reaction zone length with increasing space velocity. Upon inspection of the data and the experimental procedure, it was determined that the unregulated inlet temperature, that was not constant for all space velocities, produces a confounding effect that hinders an explicit set of conclusions from the data. It can, however, be inferred that the trend of reaction zone length increasing with space velocity is plausible. Higher space

velocity causes more active sites of the catalyst to be occupied at a given time, thus lengthening the amount of catalyst that is necessary to facilitate reactions.

Computational analyses were conducted with the acquired *in situ* data. Using the internal temperature and composition measurements, coupled with the operating parameters for each experiment (i.e. space velocity, inlet composition and furnace temperature), code was developed in EES to thermodynamically and chemically analyze the reformer. Given the data acquired, a first law, thermodynamic analysis of the operating reformer was conducted. The data exhibited elevations of normalized heat released values in the reaction zone, as well as cooling outside of the reaction zone, with increasing space velocity. These peaks in normalized heat released values increased in their location along the length of the reactor with increasing space velocity as well, with the exception of the 100k hr<sup>-1</sup> space velocity case. The axial location of the peak value in the 100k hr<sup>-1</sup> case almost directly aligned with the axial location of the peak value in the 75k hr<sup>-1</sup> case. The 100k hr<sup>-1</sup> case also exhibits the largest peak heat released value on a plot where the values are normalized by fuel flow followed by the 150k hr<sup>-1</sup> case. Both of these peaks fall outside of the expected result. The elevated methane concentration for the 150k hr<sup>-1</sup> case could potentially contributed to the corresponding elevated peak but the 100k hr<sup>-1</sup> case appears to be due to some experimental or computational error. No definitive conclusions have been made regarding the 100k hr<sup>-1</sup> and 150k hr<sup>-1</sup> cases place outside of the general trend.

This project resulted in the production of novel instrumentation that can be used to acquire *in situ* measurements of an operating fuel reformer with reliable spatial resolution. The accuracy of the instrumentation was validated, its ability to conduct the desired

analysis and acquire the desired diagnostics was demonstrated and computational analysis, with that data, to characterize the reformer and to provide possible operational and design insights was conducted. The ability to acquire measurements of this nature provides significant value in the inferences that can be made from the data acquired, as well as computational analysis of the data produced. Ultimately, it was shown that internal measurements of operating fuel processors can be acquired in a reliable fashion and, properly utilized, can provide insights that can be of value when designing and utilizing these systems.

## **6.2 Computational Challenges**

### **6.2.1 Reaction Kinetics**

The initial plan for the computational analysis component of this project was to characterize the reforming reaction mechanism. One author [4] does broach the presence of a hydrogen pyrolysis reaction taking place early on in the reaction zone. If this pyrolysis was actually taking place inside the reaction zone, the previously presented reaction mechanism, comprised of the four chemical reactions outlined in Chapter 4, would not completely characterize the chemical processes of the reformer [4,10]. Employing basic principles of chemistry that govern the rates of reaction, and the *in situ* SpaciMS species data that was acquired as presented in Chapter 4, a set of simultaneous equations was created to solve for average reaction rates across each slice of the reactor. The analysis was conducted in EES, and despite a number of efforts to simplify the problem formulation, EES could not converge on a solution. Upon discussing the challenge with Chief Scientist, Galen Fisher, of Delphi power systems, it was concluded

that the reaction mechanism was too complex to be solved by the proposed method and the Chemkin software package, developed at Sandia National Laboratories, was used to model the chemical kinetics on a micro scale.

### **6.2.2 2<sup>nd</sup> Law Analysis**

While developing the EES computational analysis tool, it was discovered that not enough operating parameters were available during the experimentation to successfully conduct thermodynamic second law analyses. Such analysis requires a control volume boundary temperature to determine internal entropy generation. The ability to acquire a temperature, precisely at the outer surface of each “slice” of the reactor vessel, does not exist but a thermal circuit analysis could be conducted given some external temperature (i.e. surface of the quartz tube). Since that data was not available, Second Law analysis was excluded.

## **6.3 Future Work**

The experimental component of this project is focused on methodology and instrumentation validation and an overall proof of concept. The experiments that were conducted and the data that was acquired validated the use of the SpaciMS and temperature acquisition mechanisms to extract *in situ* measurements, of an operating fuel reformer with fine and reliable spatial resolution. With the ability to conduct this type of analysis now in place, a plethora of other tools and a number of applications need to be inspected. Gasoline, diesel, and biofuels are just a few hydrocarbon fuels that will need to be inspected for this type of application. Automobiles and aircrafts are a potential

application sector, and power plants could possibly benefit from this type of fuel processing as well.

In the more immediate future, investigating  $C_2+$  hydrocarbons would be the most logical and necessary next step. Both olefinic and paraffinic species will be studied. These hydrocarbons with higher C content, release greater amounts of energy when undergoing conversion to produce hydrogen or synthesis gas. A scoping experiment using propane ( $C_3H_8$ ) as the feed fuel was conducted and neither the thermocouple nor the SpaciMS probe were able to withstand the extreme thermal conditions. Controlling the heat released, maximizing synthesis gas output and ensuring catalyst/reactor reliability will be integral components of the future experimental investigation. Investigations exploring the impact of a rhodium based catalyst on the impact of the methanation reaction needs to be conducted as well.

Regarding computational development, both of the points discussed in Section 6.2 have potential to add significant value to the computational analysis. Second law, thermodynamic analysis is essential in improving the efficiency of a system, thus determining areas along the reactor where the maximum amount of exergy is destroyed, provides insight on how to possibly improve its design. Quantifying chemical kinetics, especially along the reaction zone, can provide insight on how to control the occurrence of certain reactions in attempts to decrease heat loss. Varying space velocities, C:O ratios, etc. can create conditions that result in an optimal performance, minimizing heat released and maximizing overall conversion and syn gas output. Creating a tool to conduct macro level chemical kinetic analysis, along with folding second law thermodynamic analysis into the pre-existing computational tool are thus potential next steps.

Fuel processing is a technology that provides the capability to produce power in a more environmentally benign fashion than is currently employed within our pre-existing fossil fuel energy infrastructure. It has promise to improve automotive efficiency, decrease harmful NO<sub>x</sub> emissions, supply fuel for highly efficient fuel cells and pre-treat harmful exhaust. Though the promise is bright, there is still a significant amount of technological development that needs to take place before this type of fuel processor is ready for system integration. Development of this *in situ* data acquisition mechanism signifies progress in that direction, and the ability to utilize the diagnostics as demonstrated through the computational tool further substantiates the impact of this instrumentation. The novel capabilities of the SpaciMS and its supplemental instrumentation could be integral in developing fuel processing technology.

## APPENDIX A

"Dimitri Hughes"  
"Haynes Research Group"  
"Facilitated Characterization of a CPOX Fuel Reformer using In Situ Measurements"  
"Code Version B - EES Database Properties"  
"SV=150k hr-1"  
"Version 6 - 12/05/08"

PROCEDURE ARGONENTHALPY (Temp : h\_Ar)

"Argon Coefficients"

A\_1\_Ar=Lookup ('NASA Coefficients - High Temp',8,1)  
A\_2\_Ar=Lookup ('NASA Coefficients - High Temp',8,2)  
A\_3\_Ar=Lookup ('NASA Coefficients - High Temp',8,3)  
A\_4\_Ar=Lookup ('NASA Coefficients - High Temp',8,4)  
A\_5\_Ar=Lookup ('NASA Coefficients - High Temp',8,5)  
A\_6\_Ar=Lookup ('NASA Coefficients - High Temp',8,6)

$$h_{Ar} = (R \# / \text{MolarMass}(\text{Argon}) * \text{Temp}) * (A_1_{Ar} + A_2_{Ar} * \text{Temp} / 2 + A_3_{Ar} * \text{Temp}^2 / 3 + A_4_{Ar} * \text{Temp}^3 / 4 + A_5_{Ar} * \text{Temp}^4 / 5 + A_6_{Ar} / \text{Temp})$$

END

PROCEDURE CONCENTRATION (Conc\_in:Conc\_out)

IF (Conc\_in<0) THEN  
  Conc\_out=0  
ELSE  
  Conc\_out=Conc\_in  
ENDIF  
END

"Concentration Arrays"

Duplicate i=1,49

H2\_dummy[i]=Lookup ('H2 Concentration',i,1)  
H2O\_dummy[i]=Lookup ('H2O Concentration',i,1)  
Ar\_dummy[i]=Lookup ('Ar Concentration',i,1)  
CH4\_dummy[i]=Lookup ('CH4 Concentration',i,1)  
CO\_dummy[i]=Lookup ('CO Concentration',i,1)  
O2\_dummy[i]=Lookup ('O2 Concentration',i,1)  
CO2\_dummy[i]=Lookup ('CO2 Concentration',i,1)  
Position[i]=Lookup ('Position',i,1)

end

Duplicate i=1,49

CALL CONCENTRATION(H2\_dummy[i]:H2\_conc[i])  
CALL CONCENTRATION(H2O\_dummy[i]:H2O\_conc[i])  
CALL CONCENTRATION(Ar\_dummy[i]:Ar\_conc[i])  
CALL CONCENTRATION(CH4\_dummy[i]:CH4\_conc[i])  
CALL CONCENTRATION(CO\_dummy[i]:CO\_conc[i])  
CALL CONCENTRATION(O2\_dummy[i]:O2\_conc[i])  
CALL CONCENTRATION(CO2\_dummy[i]:CO2\_conc[i])  
conc\_dummy\_total[i]=sum(H2\_dummy[i],H2O\_dummy[i],Ar\_dummy[i],CH4\_dummy[i],CO\_dummy[i],O2\_dummy[i],CO2\_dummy[i])



```

    conc_total[i]=sum(H2_conc[i],H2O_conc[i],Ar_conc[i],CH4_conc[i],CO_conc[i],O2_conc[i],CO
2_conc[i])
end

```

### "System Parameters"

Count = 49

{Space Velocity or GHSV = (volumes of feed as gas at STP/hr)/(volume of the reactor or its content of catalyst)}

SV=41.6667 {SV converted to s<sup>-1</sup>} {150k hr<sup>-1</sup>}

Area\_reactor=pi\*0.01016^2

Length\_reactor=.0254[m]

Vol\_reactor=Area\_reactor\*Length\_reactor

V\_dot\_std=Vol\_reactor\*SV

T\_std=273.15[K]

P\_std = 101.325[kPa]

P\_atm=101.325[kPa]

R\_Ar=R#/MW\_Ar

temp\_limit = 1000[K]

MW\_Ar=MolarMass(Argon)

MW\_O2=MolarMass(Oxygen)

MW\_H2=MolarMass(Hydrogen)

MW\_H2O=MolarMass(Water)

MW\_CO2=MolarMass(CarbonDioxide)

MW\_CO=MolarMass(CarbonMonoxide)

MW\_CH4=MolarMass(Methane)

MW\_std=.274\*MW\_CH4+.151\*MW\_O2+(1-.274-.151)\*MW\_Ar

{This forms a temperature array}

Duplicate i= 1,49

Temp[i]=Lookup('Temperature',i,1)

MW\_actual[i]=MW\_Ar\*Ar\_conc[i]+MW\_O2\*O2\_conc[i]+MW\_H2\*H2\_conc[i]+MW\_H2O\*H2O\_
conc[i]+MW\_CO2\*CO2\_conc[i]+MW\_CO\*CO\_conc[i]+MW\_CH4\*CH4\_conc[i]

V\_dot\_actual[i]=V\_dot\_std\*((Temp[i]/T\_std)\*(P\_std/P\_atm)\*(MW\_std/MW\_actual[i]))

n\_dot\_actual[i]=((P\_atm\*V\_dot\_actual[i])/((R#)\*Temp[i]))

end

{Forms an array of enthalpies}

Duplicate i=1,49

h\_H2[i]=Enthalpy(H2,T=Temp[i])

h\_H2O[i]=Enthalpy(H2O,T=Temp[i])

h\_CH4[i]=Enthalpy(CH4,T=Temp[i])

h\_CO[i]=Enthalpy(CO,T=Temp[i])

h\_CO2[i]=Enthalpy(CO2,T=Temp[i])

h\_O2[i]=Enthalpy(O2,T=Temp[i])

CALL ARGONENTHALPY (Temp[i] : h\_Ar[i])

end

{Forms Pressure Arrays}

Duplicate i=1,49

P\_H2[i]=P\_atm\*H2\_conc[i]

```

P_H2O[i]=P_atm*H2O_conc[i]
P_Ar[i]=P_atm*Ar_conc[i]
P_CH4[i]=P_atm*CH4_conc[i]
P_CO[i]=P_atm*CO_conc[i]
P_O2[i]=P_atm*O2_conc[i]
P_CO2[i]=P_atm*CO2_conc[i]
end

```

```

{mass flow rate of each species}
{Need to determine %mass or %volume or %moles}
{Assuming %volume and correlating with Volumetric Flow Rate}

```

```

Duplicate i=1,49
  m_dot_H2[i]=n_dot_actual[i]*H2_conc[i]*MW_H2
  m_dot_H2O[i]=n_dot_actual[i]*H2O_conc[i]*MW_H2O
  m_dot_Ar[i]=n_dot_actual[i]*Ar_conc[i]*MW_Ar
  m_dot_CH4[i]=n_dot_actual[i]*CH4_conc[i]*MW_CH4
  m_dot_CO2[i]=n_dot_actual[i]*CO2_conc[i]*MW_CO2
  m_dot_O2[i]=n_dot_actual[i]*O2_conc[i]*MW_O2
  m_dot_CO[i]=n_dot_actual[i]*CO_conc[i]*MW_CO
  m_dot_total[i]=sum(m_dot_H2[i],m_dot_H2O[i],m_dot_Ar[i],m_dot_CH4[i],m_dot_CO2[i],m_dot_O2[i],m_dot_CO[i])
end

```

```

{
{Carbon Atom Trace}
Duplicate i=1,49
C_n_dot[i]=n_dot_actual[i]*(CH4_conc[i]+CO2_conc[i]+CO_conc[i])
O_n_dot[i]=n_dot_actual[i]*(2*O2_conc[i]+2*CO2_conc[i]+CO_conc[i])
H_n_dot[i]=n_dot_actual[i]*(2*H2_conc[i]+2*H2O_conc[i]+4*CH4_conc[i])
end}

```

```

{Calculating Enthalpy transfered}

```

```

Duplicate i=1,49
  H_total_out[i]=m_dot_H2[i]*h_H2[i]+m_dot_H2O[i]*h_H2O[i]+m_dot_CH4[i]*h_CH4[i]+m_dot_CO2[i]*h_CO2[i]+m_dot_O2[i]*h_O2[i]+m_dot_CO[i]*h_CO[i]+m_dot_Ar[i]*h_Ar[i]
end

```

```

Duplicate i=2,49
  Q_dot_total2[i]=H_total_out[i-1]-H_total_out[i]
  Q_dot_total3[i]=H_total_out[i]-H_total_out[i-1]
end

```

```

{
{calculating total heat in the reactor}

```

```

Duplicate i=2,49
  Q_dot_H2[i]=m_dot_H2[i]*(h_H2[i]-h_H2[i-1])
  Q_dot_H2O[i]=m_dot_H2O[i]*(h_H2O[i]-h_H2O[i-1])
  Q_dot_CH4[i]=m_dot_CH4[i]*(h_CH4[i]-h_CH4[i-1])
  Q_dot_CO2[i]=m_dot_CO2[i]*(h_CO2[i]-h_CO2[i-1])
  Q_dot_O2[i]=m_dot_O2[i]*(h_O2[i]-h_O2[i-1])
  Q_dot_CO[i]=m_dot_CO[i]*(h_CO[i]-h_CO[i-1])
  Q_dot_Ar[i]=m_dot_Ar[i]*(h_Ar[i]-h_Ar[i-1])
  Q_dot_total1[i]=sum(Q_dot_H2[i],Q_dot_H2O[i], Q_dot_CH4[i], Q_dot_CO2[i], Q_dot_O2[i],
Q_dot_CO[i], Q_dot_Ar[i])
end}

```

## APPENDIX B

### Ideal Gas Approximation Validation

All of the constituents present in the system, with the exception of water, readily characterized under the ideal gas assumption. In order to validate the ideal gas assumption for H<sub>2</sub>O, its compressibility factor was calculated under an array of the most extreme thermal and pressure conditions that could be present in the reactor. The equation used to calculate the compressibility factor, as provided by Moran and Shapiro [15], is illustrated in Equation 5.1. “P” represents the partial pressure of the water vapor;  $v$  represents the specific volume of the water vapor at the given conditions; R is the water vapor gas constant and T is the absolute temperature of the water vapor.

$$Z = \frac{Pv}{RT} \quad (5.1)$$

The concentration of water vapor inside the reactor ranged from 1 – 4% and with the pressure inside the reactor being nearly atmospheric, the partial pressure of water vapor ranged between .01 atm and .04 atm or 1.013 kPa and 4.053 kPa. The maximum measured temperature inside the reaction zone was 1300 K and the minimum temperature within the reactor is 700K.

**Table B.1: Compressibility Factor Solutions**

	700K	1300K
v_H20_1	318.8	592.1
v_H20_2	159.4	296.1
v_H20_3	106.3	197.4
v_H20_4	79.71	148
v_water_1	318.8	592.1
v_water_2	159.4	296.1
v_water_3	106.3	197.4
v_water_4	79.71	148
Z_1_H2O	1	1
Z_2_H2O	1	1
Z_3_H2O	1	1
Z_4_H2O	1	1
Z_1_water	1	1
Z_2_water	1	1
Z_3_water	1	1
Z_4_water	1	1

EES code was developed to calculate the compressibility factor of water vapor at both the high and low temperature (low temperature = 700K, high temperature = 1300K) and pressures (low pressure = .01 atm , high pressure = .04 atm) in increments of .01 atm. EES has thermophysical properties for H2O, based upon the ideal gas and real gas equations of state.

The code is designed to calculate the compressibility factor with property values being evaluated using both the ideal gas and real gas equations of state. In addition to calculating the compressibility factors for these conditions, Table 5.1 also provides a comparison between ideal and real gas specific volume values. The variables of the form  $Z_{\text{number}}_{\text{H2O}}$  signify the use of the ideal gas equation of state and the variables of the general form  $Z_{\text{number}}_{\text{water}}$  signify the use of the real gas equation of state. For all of the prescribed conditions, the compressibility ratio approached unity. The ideal gas

assumption is valid for water vapor in this application and the universal ideal gas equation of state and all other subsequent assumptions can be applied to the analysis of water vapor.

## APPENDIX C

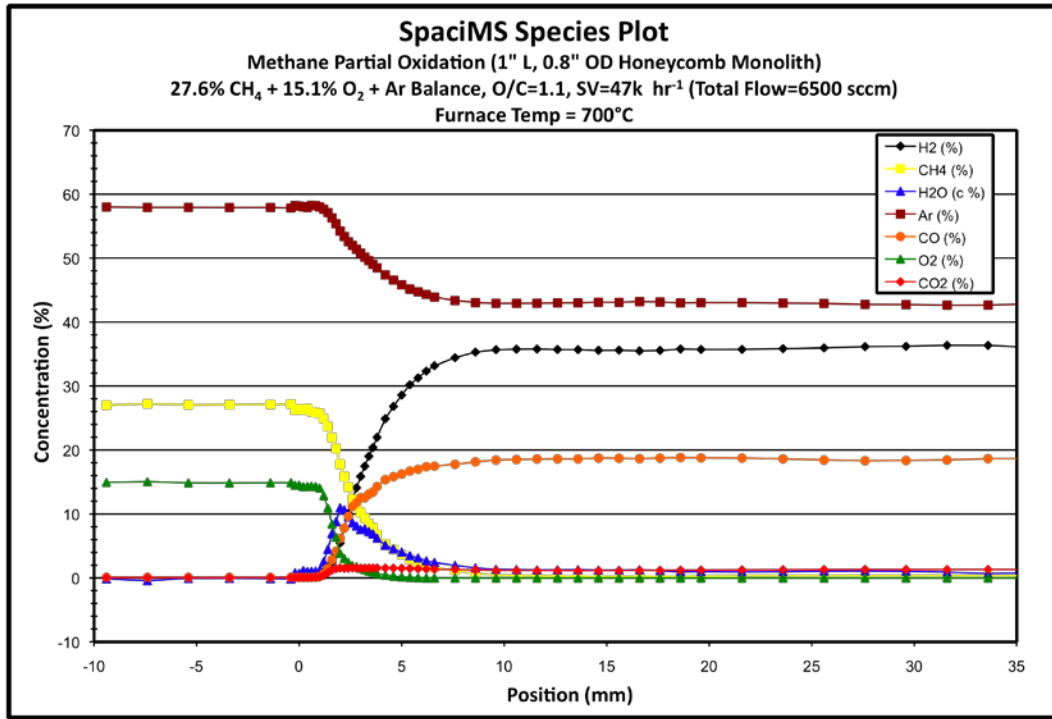


Figure C.1 Species composition as a function of position for 47k hr-1 experiment

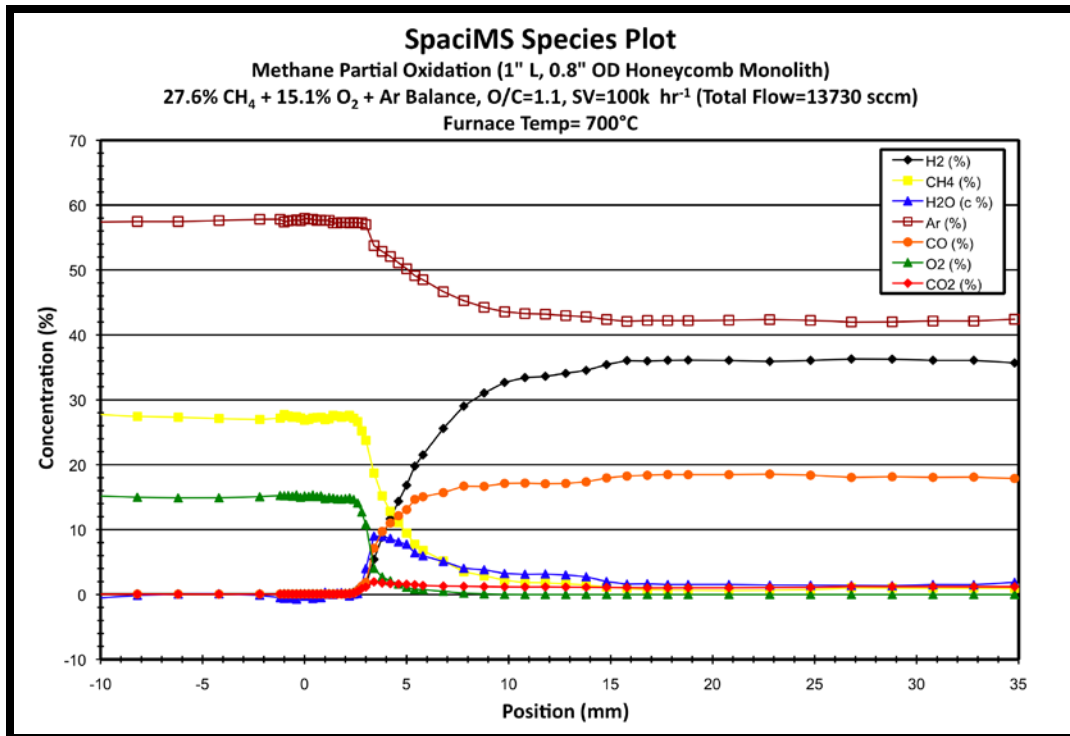


Figure C.2 Species composition as a function of position for 100k hr-1 experiment

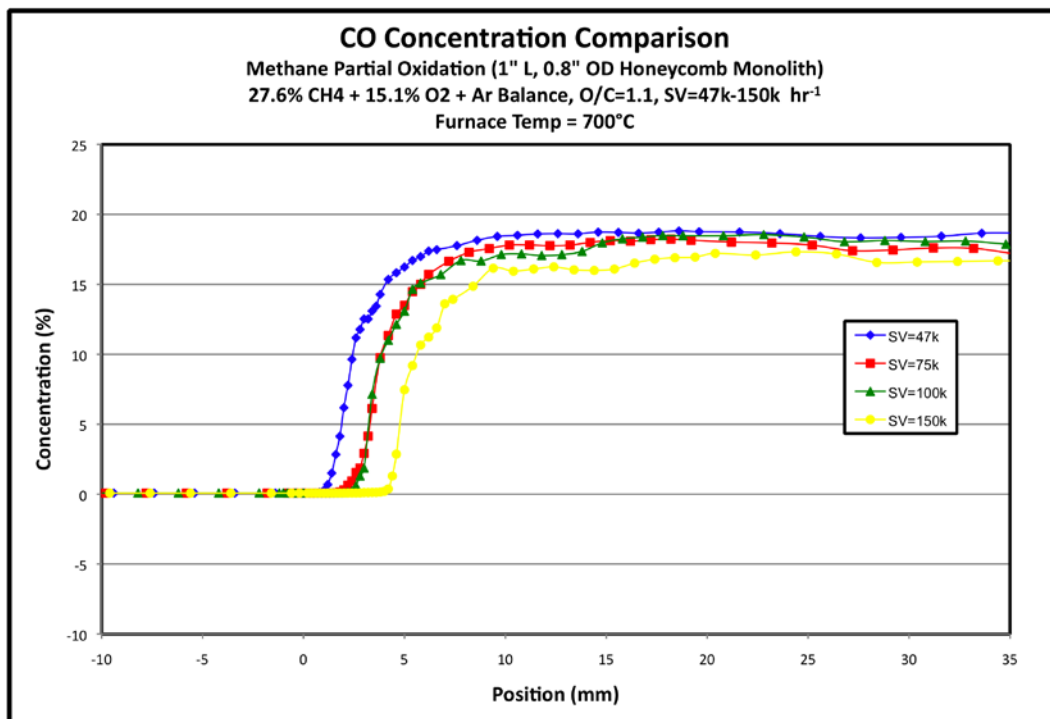


Figure C.3 Carbon Monoxide concentration as a function of position across all space velocities (Note: Units of space velocity are hr<sup>-1</sup>)

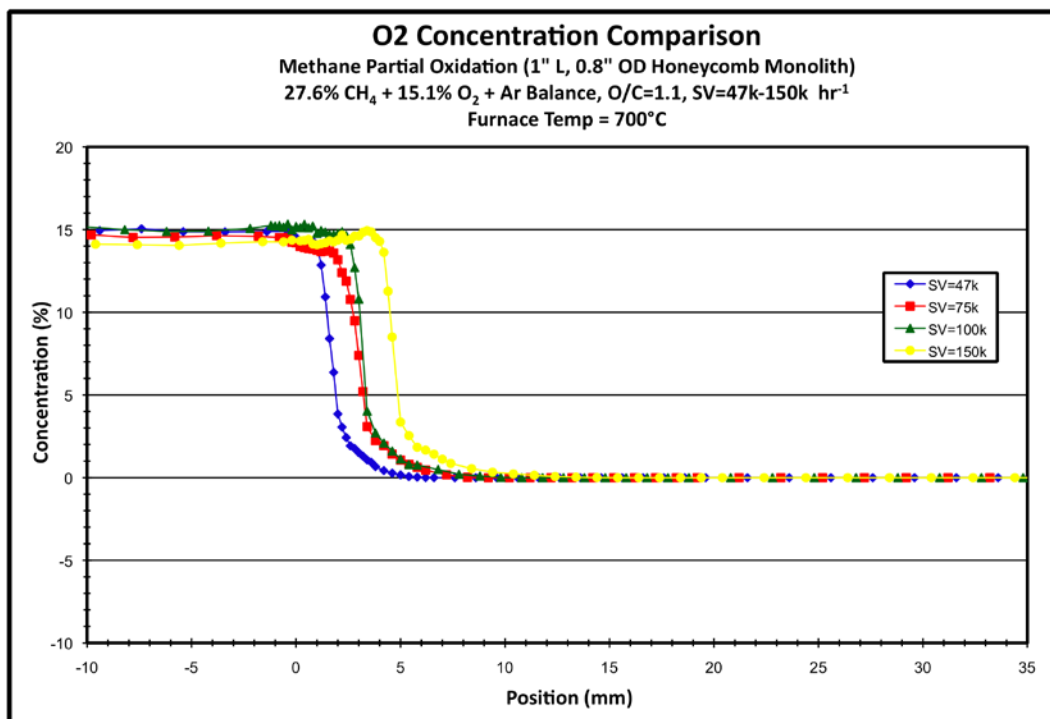


Figure 4.5 Oxygen concentration as a function of position across all space velocities (Note: Units of space velocity are hr<sup>-1</sup>)

## REFERENCES

1. U.S. DOE Laboratory. (2004). *Fuel Cell Handbook, 7th Ed.* Morgantown, WV: U.S. DOE.
2. Larminie, J., & Dicks, A. (2003). *Fuel Cell Systems Explained, 2nd. Ed.* John Wiley & Sons, Ltd.
3. Horn, R., Williams, K. A., Degenstein, N. J., & Schmidt, L. D. (2006). Syngas by Catalytic Partial Oxidation of Methane on Rhodium: Mechanistic Conclusions from Spatially Resolved Measurements and Numerical Simulations. *Journal of Catalysis* , 242, 92-102.
4. Kikas, T., Bardenshteyn, I., Williamson, C., Ejimofor, C., Puri, P., & Fedorov, A. G. (2003). Hydrogen Production in a Reverse-Flow Autothermal Catalytic Microreactor: From Evidence of Performance Enhancement to Innovative Reactor Design. *Industrial and Engineering Chemistry Journal* , 42, 6273-6279.
5. Choi, J.-S., Partridge, W. P., & Daw, C. S. (2005). Spatially Resolved in situ Measurements of Transient Species Breakthrough During Cyclic, Low-Temperature Regeneration of a Monolithic Pt/K/Al<sub>2</sub>O<sub>3</sub> NO<sub>x</sub> Storage-Reduction Catalyst. *Applied Catalysis A:General* , 293, 24-40.
6. Kreith, F., & West, R. (2004). Fallacies of a Hydrogen Economy: A Critical Analysis of Hydrogen Production and Utilization. *Journal of Energy Resources Technology* , 126, 249-257.
7. Sampara, C., Depcik, C., & Assanis, D. (2005). Framework for Modeling the Components of a Fuel Processing System for Fuel Cell Applications. *2005 ASME International Mechanical Engineering Congress and Exposition* (pp. 1-11). Orlando, FL: ASME.
8. Chaniotis, A. K., & Poulidakos, D. (2005). Modeling and Optimization of Catalytic Partial Oxidation Methane Reforming for Fuel Cells. *Journal of Power Sources* , 142, 184-193.
9. Lutz, A. E., Bradshaw, R. W., Bromberg, L., & Rabinovich, A. (2004). Thermodynamic Analysis of Hydrogen Production by Partial Oxidation Reforming. *International Journal of Hydrogen Energy* , 29, 809-816.
10. Kaisare, N. S., Lee, J. H., & Fedorov, A. G. (2005). Hydrogen Generation in a Reverse-Flow Microreactor: 1. Model Formulation and Scaling. *AIChE Journal* , 51 (8), 2254-2264.
11. Kaisare, N. S., Lee, J. H., & Fedorov, A. G. (2005). Hydrogen Generation in a Reverse-Flow Microreactor: 2. Simulation and Analysis. *AIChE Journal* , 51 (8), 2265-2272.



12. Kaisare, N. S., Lee, J. H., & Fedorov, A. G. (2005). Operability Analysis and Design of a Reverse-Flow Microreactor for Hydrogen Generation via Methane Partial Oxidation. *Industrial and Engineering Chemistry Research* , 44, 8823-8833.
13. Bharadwaj, S. S., & Schmidt, L. D. (1995). Catalytic Partial Oxidation of Natural Gas to Syngas. *Fuel Processing Technology* , 109-127.
14. Partridge, W. P., Toops, T. J., Green, J. B., & Armstrong, T. R. (2006). Intra-Fuel Cell Stack Measurements of Transient Concentration Distributions. *Journal of Power Sources* , 160, 454-461.
15. Omega Engineering (2009). *Omega Handbook*. Stamford, CT: Omega Engineering, Inc.
16. Moran, J., & Shapiro, H. N. (2005). *Fundamentals of Engineering Thermodynamics*. Wiley & Sons.
17. Bodke, A. S., Bharadwaj, S. S., & Schmidt, L. D. (1998). The Effect of Ceramic Supports on Partial Oxidation of Hydrocarbons over Noble Metal Coated Monoliths. *Journal of Catalysts* , 179, 138-149.
18. Nadal, M., & Barbir, F. (1996). Development of a Hybrid Fuel Cell/Battery Powered Electric Vehicle. *International Journal of Hydrogen Energy* , 21 (6), 497-505.
19. Parks, J., Huff, S., Pihl, J., Choi, J.-S., & West, B. (2005). Nitrogen Selectivity in Lean NO<sub>x</sub> Trap Catalysts with Diesel Engine In-Cylinder Regeneration. *SAE International* .
20. Partridge, W. P., Lewis, S. A., Ruth, M. J., Muntean, G. G., Smith, R. C., & Stang, J. H. (2001). Resolving EGR Distribution and Mixing. *SAE* .
21. Partridge, W. P., Storey, J. M., Lewis, S. A., Smithwick, R. W., DeVault, G. L., Cunningham, M. J., et al. (2000). Time-Resolved Measurements of Emission Transients by Mass Spectrometry. *Society of Automotive Engineers*. SAE.
22. Pukrushpan, J. T., Stefanopoulou, A. G., Varigonda, S., & Pedersen, L. M. (2005). Control of Natural Gas Catalytic Partial Oxidation for Hydrogen Generation in Fuel Cell Applications. *IEEE Transactions on Control Systems Technology* , 13 (1), 3-14.
23. Yokoo, M., Take, T., & Ohtsu, S. (2004). Performance Evaluation of SOFC Systems Using Electrochemical Partial Oxidation of Methane. *Electrical Engineering in Japan* , 147 (4), 466-474.
24. Turns, S. R. (2000). *An Introduction to Combustion: Concepts and Applications*, 2nd Ed. Mc-Graw Hill.

25. Perry, R. H., & Green, W. (1997). *Perry's Chemical Engineer's Hand Book, 7th Ed.* New York: McGraw-Hill.
26. Reid, R. C., Prausnitz, J. M., & Poling, B. E. (1987). *The Properties of Gases & Liquids, 4th Ed.* McGraw-Hill Inc.
27. Incropera, F. P., & DeWitt, D. P. (2002). *Fundamentals of Heat and Mass Transfer, 5th Ed.* John Wiley & Sons, Inc.